Lithos xxx (2011) xxx–xxx

Contents lists available at ScienceDirect

Lithos

journal homepage: www.elsevier.com/locate/lithos

High-Cr and high-Al chromitites from the Sagua de Tánamo district, Mayarí-Cristal ophiolitic massif (eastern Cuba): Constraints on their origin from mineralogy and geochemistry of chromian spinel and platinum-group elements

J.M. González-Jiménez [a,*], J.A. Proenza [b], F. Gervilla [c], J.C. Melgarejo [b], J.A. Blanco-Moreno [d], R. Ruiz-Sánchez [e], W.L. Griffin [a]

[a] GEMOC ARC National Key Centre, Department of Earth and Planetary Sciences, Macquarie University, Sydney, NSW 2109, Australia
[b] Departament de Cristal·lografia, Mineralogia i Dipòsits Minerals, Universitat de Barcelona, Martí i Franquès s/n, 08028, Barcelona, Spain
[c] Departamento de Mineralogía y Petrología and Instituto Andaluz de Ciencias de la Tierra (Universidad de Granada-CSIC), Facultad de Ciencias, Avda. Fuentenueva s/n, 18002 Granada, Spain
[d] Departamento de Geología, Instituto Superior Minero Metalúrgico de Moa, Las Coloradas s/n, 83320, Moa, Holguín, Cuba
[e] Empresa Geominera de Oriente, Carretera de Siboney s/n, Santiago de Cuba, Cuba

ARTICLE INFO

Article history:
Received 13 May 2010
Accepted 28 January 2011
Available online xxxx

Keywords:
Ophiolitic chromitite
High-Cr and high-Al chromian spinel
Platinum-group elements
Platinum-group minerals
Cuba

ABSTRACT

Several chromitite bodies of variable sizes are hosted in dunite-harzburgite of the small (<3 km) mining district of Sagua de Tánamo, in the Mayarí-Cristal ophiolitic massif, eastern of Cuba. The chromian spinel in these bodies displays a large range in Cr# (Cr/Cr + Al) atomic ratio from 0.74 to 0.45. In high-Cr chromitites, Cr# and Ti contents increase from harzburgite to dunite, to chromitite. A roughly opposite trend of variation in Cr# is observed in high-Al chromitites, although in this case Ti distributes randomly. The differences in the type of chromian spinel (i.e., high-Cr or high-Al) in the chromitite coincide with a different behavior of the platinum-group elements (PGE). Whereas high-Cr chromitites are rich in PGE and contain abundant grains of platinum-group minerals (PGM), high-Al chromitites are systematically poor in PGE and in PGM. The calculated melts in equilibrium with chromian spinel of high-Cr chromitite are island arc thoeliites (IAT) with boninitic affinity whereas those in equilibrium with chromian spinel of high-Al chromitites are back-arc basin basalts (BABB). The formation of high-Cr chromitites is interpreted as a result of the extensive reaction of harzburgite with migrating island arc tholeiite melts of boninitic affinity. Melt–rock reaction produces boninitic melts with variable composition and porous dunitic channels in which the mixing/mingling of melts promotes crystallization of mononomineralic high-Cr chromian spinel. In contrast, high-Al chromitites formed by the mixing/mingling of BABB melts within conduits not in equilibrium with dunite. Percolation of primitive BABB melts through pre-existing dunite dissolved olivine, producing melt conduits in which BABB melts mixed and formed high-Al chromian spinel. The higher PGE and PGM in high-Cr chromitites is not only a function of the degree of partial melting but is linked to interaction between the migrating melt and mantle harzburgite during the formation of the chromitite. The coexistence of both types of chromitites in one small mining district reflects the temporal and/or spatial variations of separate melt intrusions emplaced in different subarc mantle domains during the opening of a back-arc basin in a supra-subduction zone environment.

1. Introduction

Chromitite bodies of variable size occur at different levels within the mantle harzburgite section of the Mayarí-Cristal ophiolite massif and, in the mantle–crust transition zone of the Moa-Baracoa massif, both parts of the Mayarí-Baracoa Ophiolitic Belt, eastern Cuba (Murashko and Lavandero, 1989; Proenza et al., 1999; Gervilla et al., 2005). These chromitites were grouped by Proenza et al. (1999) into three mining districts, according to the composition of chromite in the chromitite: (1) the Mayarí district (high-Cr); (2) the Sagua de Tánamo district (high-Cr and high-Al); and the (3) Moa-Baracoa district (high-Al). The Mayarí and Sagua de Tánamo districts are located in the western and easternmost part of the Mayarí-Cristal massif respectively, whereas the Moa-Baracoa district comprises the whole Moa-Baracoa massif.

About 35 chromitite bodies (25 high-Cr and 10 high-Al) were described in the small district of Sagua de Tánamo (Thayer, 1942; Murashko and Lavandero, 1989; Kovács et al., 1997). Gervilla et al.

* Corresponding author.
E-mail addresses: jose.gonzalez@mq.edu.au (J.M. González-Jiménez), japroenza@ub.edu (J.A. Proenza), gervilla@ugr.es (F. Gervilla), bill.griffin@mq.edu.au (W.L. Griffin).

0024-4937/$ – see front matter © 2011 Elsevier B.V. All rights reserved.
doi:10.1016/j.lithos.2011.01.016

(2005) interpreted Sagua de Tánamo as a continuous transition between the Mayarí district, (beneath a paleo-arc), and the Moa-Baracoa district (back-arc basin). However, new geochemical (Marchesi et al., 2006, 2007; Proenza et al., 2006) and Os-isotope data (Frei et al., 2006; Marchesi et al., 2010) in the area have supplied a better platform for addressing some remaining questions with respect to the origin of these chromitites and their relationships with their host rocks, their tectonic setting, and their broader significance with respect to the spatial coexistence of high-Cr and high-Al chromitites observed in other ophiolitic complexes. The Sagua de Tánamo chromitites are of particular interest because they are one of the few examples where high-Cr and high-Al chromitites outcrop within the same ultramafic massif, and over a short distance (<3 km). In this contribution we re-examine eight previously known chromitite bodies (five high-Cr and three high-Al), and provide data for other two chromitite bodies not previously investigated (one high-Cr chromitite [i.e., Tres Amigos] and one high-Al chromitite [i.e., Demajagua]). These data comprise chromian spinel composition, and the mineralogy and geochemistry of the platinum-group elements (PGE).

2. Geological setting and chromitite

The Northern Cuban Ophiolite Belt comprises a set of strongly faulted ultramafic, plutonic, volcanic and sedimentary mélange complexes that define a discontinuous W–E belt in northern Cuba (Fig. 1, inset). This Ophiolitic Belt is part of the Cuban fold belt, a tectonic unit made up of deformed and metamorphosed nappes accreted during late Cretaceous to earliest Paleocene times (e.g., Iturralde-Vinent et al., 2006). The easternmost branch of this ophiolitic belt is known as the Mayarí-Baracoa Ophiolitic Belt (Fig. 1). This belt is tectonically emplaced on subduction-related metamorphic mélanges containing high-pressure tectonic blocks (i.e., the Sierra del Convento mélange [García-Casco et al., 2006, 2008; Lázaro et al., 2009] and the La Corea Melánge [Blanco-Quintero et al., 2011]). The ophiolite and the metamorphic complex have been thrust over Cretaceous volcanic arc complexes, with formations that have distinct geochemical signatures including tholeiitic, boninitic and calc-alkaline (Proenza et al., 2006). These signatures indicate different stages of the evolution of an island arc from early Cretaceous (Aptian–Albian) to late Cretaceous (mid-Campanian), according to paleontological data (Iturralde-Vinent et al., 2006). Obduction occurred during Late Cretaceous (i.e., Maastrichtian times ca. 65 Ma) to earliest Paleocene time, and is recorded by olistrostromic units that are overthrust by the above-mentioned units (Iturralde-Vinent et al., 2006).

The Mayarí-Baracoa Ophiolitic Belt consists of two large massifs (Proenza et al., 1999; Marchesi et al., 2006): the Moa-Baracoa massif to the east and the Mayarí-Cristal to the west (Fig. 1). The Moa-Baracoa massif is made up of a section (>2.2 km thick) of mantle tectonite harzburgite with subordinate dunite, and a Moho transition zone (MTZ) overlain by layered gabbros of the lower oceanic crust (ca 500 m thick). The Mayarí-Cristal massif is essentially a peridotite massif (>5 km thick) made up of highly serpentinized harzburgite tectonite hosting minor subconcordant dunite, both intensively altered in an ocean-floor environment (Proenza et al., 2003). Peridotites are locally cut by gabbroic and pyroxenitic dykes of IAT affinity (Marchesi et al., 2006). Fonseca et al. (1985) have described a sheeted-dyke complex in the northwestern part of the body, but Marchesi et al. (2006) argue that this is a subvolcanic complex made up of massive microgabbros in tectonic contact with the

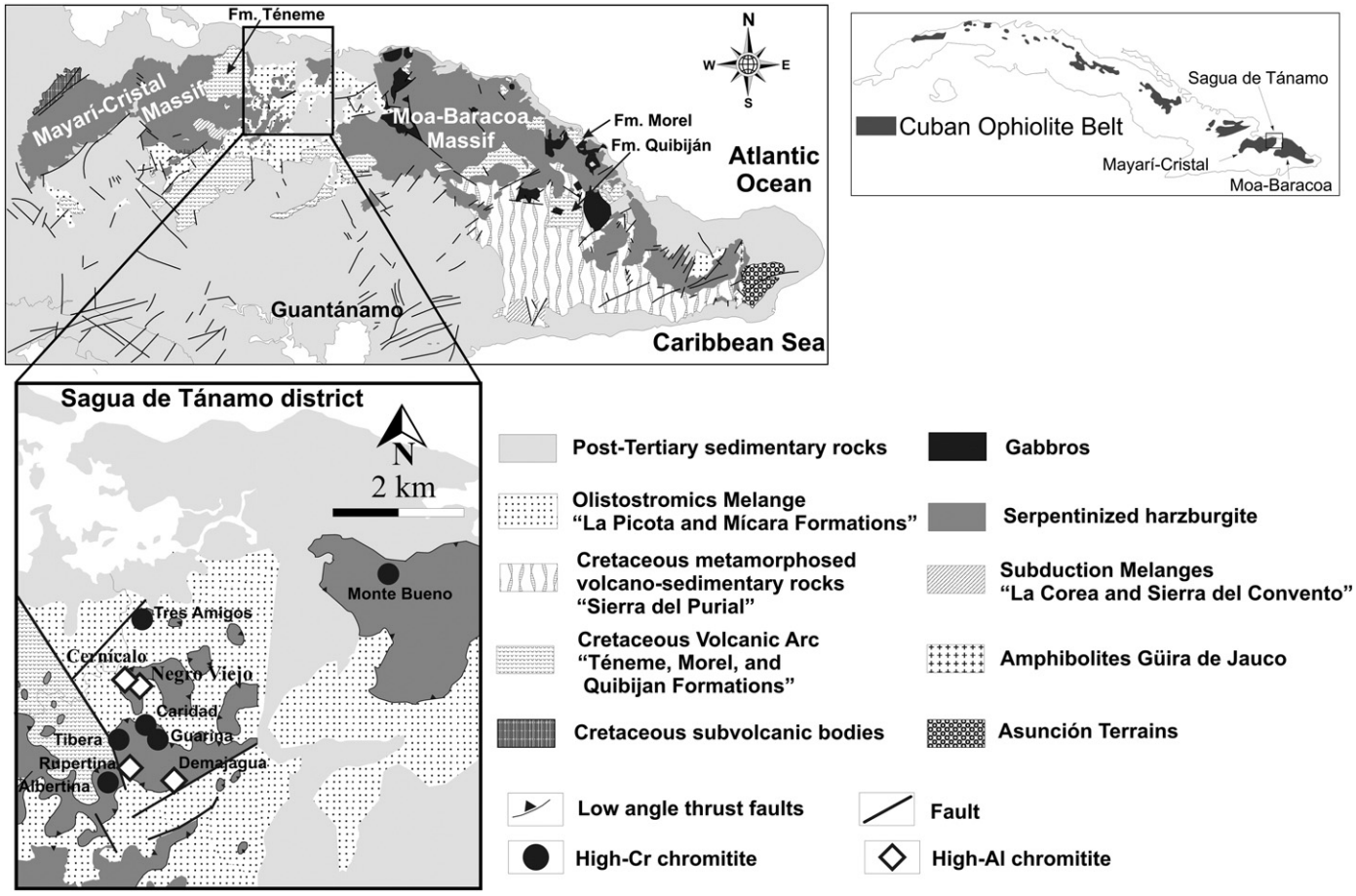

Fig. 1. Location of the Sagua de Tánamo district in the Mayarí-Baracoa ophiolitic belt and in eastern Cuba, and simplified geological map with location of the studied chromitites.

Please cite this article as: González-Jiménez, J.M., et al., High-Cr and high-Al chromitites from the Sagua de Tánamo district, Mayarí-Cristal ophiolitic massif (eastern Cuba): Constraints on..., Lithos (2011), doi:10.1016/j.lithos.2011.01.016

harzburgite tectonites. Marchesi et al. (2006, 2007) interpreted the Moa-Baracoa massif as a portion of MORB-like lithosphere located near a Caribbean back-arc paleo-spreading ridge, and regard the Mayari-Cristal massif as a piece of transitional (MORB to IAT) back-arc mantle located closer to the Greater Antilles paleo-island arc than Moa-Baracoa.

The Sagua de Tánamo district is located in the easternmost part of the Mayarí-Cristal massif (Proenza et al., 1999) (Fig. 1). The geology of the district is dominated by highly serpentinized mantle dunite and harzburgite with tectonite structure, which are tectonically emplaced on the La Corea mélange, and the Late Cretaceous arc-related volcanic rocks of Téneme Formation and the Maastrichtian–Danian olistostromic synorogenic rocks of Micara and La Picota formations (Fig. 1) (Proenza et al., 2006; Marchesi et al., 2006, 2007; Blanco-Quintero et al., 2011). The tectonics of the area are complex and peridotites form thrust slices interbedded within the mélange zone and volcanic arc rocks (Iturralde-Vinent et al., 2006). According to Iturralde-Vinent et al. (2006), based on paleontological dating, the age of the Téneme Formation is Turonian to early Coniacioan. Téneme basaltic rocks are low-Ti island arc tholeiites with boninitic affinity, and have been interpreted as part of a nascent primitive island arc (Proenza et al., 2006).

Chromitites of both high-Cr and high-Al varieties occur interspersed within a narrow zone less than 3 km long (Fig. 1). They are typical podiform chromitites with lenses of variable sizes (30–40 m long, 10–20 m wide, 1–3 m thick), and are both concordant and discordant with the foliation of the host harzburgite. The Sagua de Tánamo chromitites, like other ophiolitic chromitites, are separated from the host harzburgite by dunite envelopes of variable thickness. Usually the contact between chromitite and dunite is gradual, defined by a zone of disseminated chromitite. The thickness of the dunite envelope correlates with the Cr_2O_3 content of the spinel in the chromitite; high-Cr chromitites tend to exhibit thicker dunite envelopes than high-Al ones. Some of the high-Cr chromitites (i.e., Guarina, Tibera, Albertina) and one high-Al chromitite (i.e., Cernícalo) host lenses, or cross-cutting dykes of fine to coarse-grained amphibole-bearing gabbro. At the hand-specimen scale, chromitite samples in contact with the gabbros show large amounts of interstitial amphibole. Identical amphibole-bearing gabbros occur away from the chromitites, in the host harzburgite.

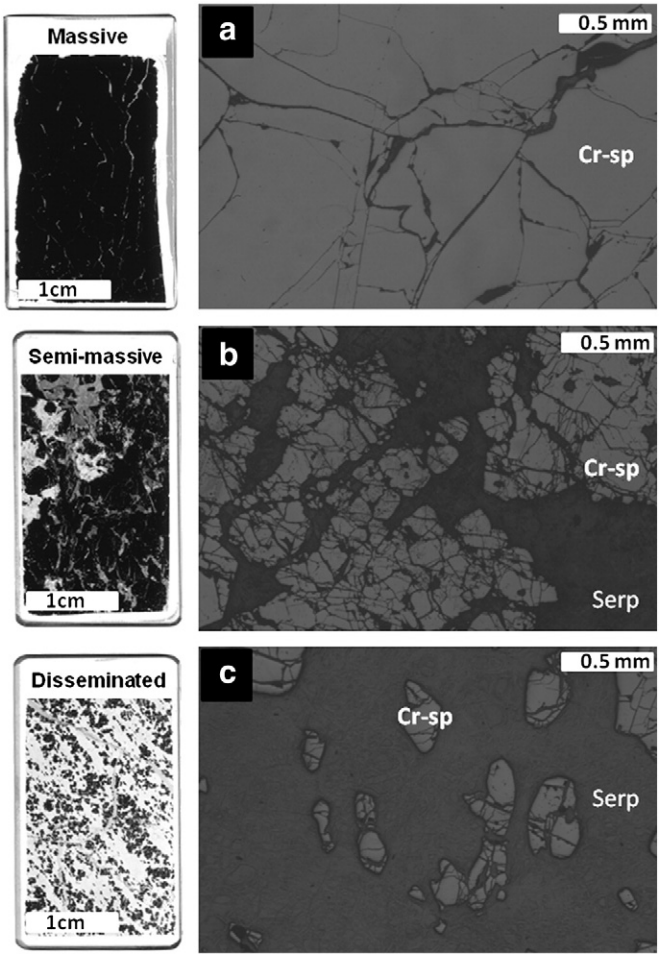

Fig. 2. Photographs of thin sections of chromitite and photomicrographs (reflected light) showing main textural types in the Sagua de Tánamo chromitites. (a) Massive chromitite from the high-Cr chromitite of Caridad. (b) Semi-massive chromitite from the high-Cr chromitite of Guarina. (c) Disseminated chromitite from the high-Al chromitite of Negro Viejo. Keys: Cr-sp: chromian spinel, Serp: serpentine.

3. Petrography

3.1. Chromitite

Chromitite texture is predominantly massive, but semi-massive disseminated and banded ores are common near the contacts with the enclosing dunite. Massive chromitite (>85% chromian spinel) is composed of coarse chromian spinel (Fig. 2a). Semi-massive (30–85% chromian spinel) and disseminated chromitite (≤30% chromian spinel) have smaller, and more subhedral crystal of chromian spinel than the massive chromitite (Fig. 2b and c). Banded chromitite consists of layers of chromian spinel (up to 5 cm thickness) and serpentinite. Most chromitite samples exhibit pull-apart fractures, and late shearing and faulting produced mylonitic, and cataclastic textures. Some grains of chromian spinel show rims of ferrian chromian spinel of variable thickness which are associated with fractures penetrating the chromian spinel.

Chromian spinel grains in chromitites contain inclusions of pyroxenes and rarely amphibole and olivine. These silicates occur either as single isolated crystals (<20 μm across) or in some cases in multiphase grains with platinum-group minerals (PGM) or base-metal sulfides (BMS). Because of the extensive sea-floor serpentinization (Proenza et al., 2003) only a few relict cores of pyroxenes and amphiboles were available for analysis. Interstitial amphibole is in direct contact with chromian spinel only in chromitite samples associated with gabbros. In the altered silicate matrix and fractures penetrating the chromian spinel grains secondary silicate grains are accompanied by secondary PGM and BMM.

3.2. Dunite and harzburgite

Dunite envelopes around the chromitite bodies are up to 3 m thick. Olivine is transformed to lizardite but minor antigorite is also present. The dunite contains more than 2% chromian spinel. According to the morphological definition of Matsumoto and Arai (2001) the chromian spinel in dunite enclosing high-Cr chromitites is predominantly anhedral (Fig. 3a–b) whereas chromian spinels in dunite hosting high-Al chromitites, which are smaller, may be subhedral or euhedral (Fig. 3c and d). Despite the strong serpentinization, chromian spinel shows either no, or very thin, ferrian chromite alteration rims. The latter are exclusively associated with late fractures cross-cutting the grains (Fig. 3b and d).

Harzburgite displays a porphyroclastic texture; it is clinopyroxene-poor and contains ubiquitous amphibole. Olivine is transformed to a lizardite-magnetite assemblage displaying mesh textures, and orthopyroxene is pseudomorphed by bastite. The harzburgite contains chromian spinel but in lower proportions than the dunite (<2 vol.%). The morphological patterns of chromian spinel are identical to those observed in the dunite. Thus, whereas chromian spinel in harzburgite hosting high-Cr chromitites is vermicular (i.e., anhedral) (Fig. 3e and f), chromian spinel in harzburgite enclosing

Please cite this article as: González-Jiménez, J.M., et al., High-Cr and high-Al chromitites from the Sagua de Tánamo district, Mayarí-Cristal ophiolitic massif (eastern Cuba): Constraints on..., Lithos (2011), doi:10.1016/j.lithos.2011.01.016

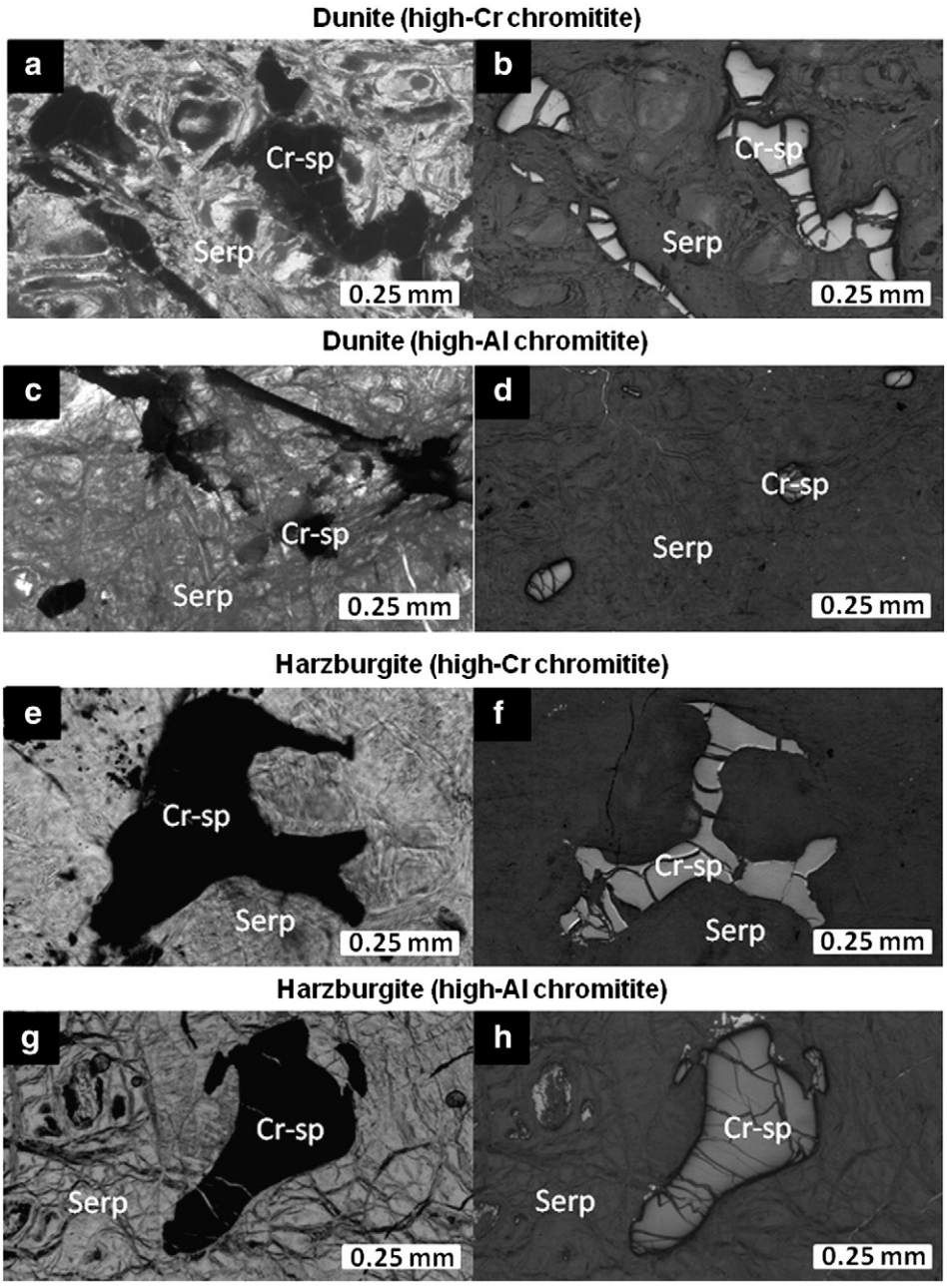

Fig. 3. Photomicrographs (transmitted right side and reflected light left side) of chromian spinel in dunite and harzburgite enclosing the Sagua de Tánamo chromitites. (a–b) irregular chromian spinel in dunite hosting the high-Cr chromitite of Caridad. (c–d) euhedral chromian spinel in dunite hosting the high-Al chromitite of Negro Viejo. (e–f) vermicular chromian spinel in harzburgite hosting the high-Cr chromitite of Caridad. (g–h) subhedral chromian spinel in harzburgite hosting the high-Al chromitite of Rupertina.

high-Al chromitites is predominantly subhedral (Fig. 3g and h). The chromian spinel in harzburgite is virtually unaltered, and only some grains exhibit narrow rims of ferrian chromite associated with fractures penetrating the grains (Fig. 3f and h).

4. Analytical techniques

Polished thin-sections were studied under reflected light at the Geochemical Analysis Unit (GAU) at GEMOC, Macquarie University, by Environmental Scanning Electron Microscopy (ESEM) at the Centro Andaluz de Medio Ambiente (University of Granada-Junta de Andalucía) and by Field Emission Scanning Electron Microscopy (FE-SEM) at the Centro de Instrumentación Científica (University of Granada), to characterize chromitite petrography and to locate platinum-group mineral (PGM), base-metal minerals (BMM), and silicate inclusions in chromitite. The analyses of these minerals were obtained using a four-channel CAMECA SX50 electron microprobe at the Serveis Cientificotècnics of the University of Barcelona. The analytical conditions were: 20 kV accelerating voltage, 20 nA beam current, 2 μm beam diameter and counting time of 10 s per element. Two different routines were performed: one to analyze chromian spinel and silicate, and a second to analyze PGM and BMM. In both cases, calibrations were performed using natural and synthetic standards. The standards used for chromite and silicate analyses were chromite (for Cr, Al and Fe), periclase (for Mg), rhodonite (for Mn), rutile (for Ti), NiO (for Ni) and metallic V. The chemical data on chromian spinel were stoichiometrically recalculated in order to distinguish FeO from Fe_2O_3 according to Carmichael's (1967) procedure. The standards used for PGM and BMM analyses were pure metals for Os, Ir, Ru, Rh,

Please cite this article as: González-Jiménez, J.M., et al., High-Cr and high-Al chromitites from the Sagua de Tánamo district, Mayarí-Cristal ophiolitic massif (eastern Cuba): Constraints on..., Lithos (2011), doi:10.1016/j.lithos.2011.01.016

Table 1
Representative electron-microprobe analyses of chromian spinel from chromitites of the Sagua de Tánamo district.

	High-Cr chromitites						High-Al chromitites			
Sample	TA-1	G-1	MB-1	SI-100	Ti-1	A-1A	NV-101	DEM-1	C-3	RU-1
TiO_2	0.10	0.21	0.28	0.29	0.39	0.32	0.10	0.20	0.19	0.15
Al_2O_3	14.39	13.23	15.88	17.15	18.90	20.05	21.23	22.95	24.37	30.14
V_2O_3	0.12	0.29	0.06	0.15	0.12	0.14	0.16	0.26	0.12	0.13
Cr_2O_3	55.89	54.95	53.04	52.33	49.16	50.02	47.61	45.96	44.58	37.89
Fe_2O_3	2.84	2.65	2.51	1.78	2.23	2.36	3.17	1.80	3.05	3.01
MgO	13.21	10.60	12.66	13.44	13.15	14.25	13.91	13.58	15.41	16.85
MnO	0.25	bdl	0.15	bdl	bdl	0.26	bdl	0.21	bdl	0.14
FeO	14.25	17.97	15.19	14.20	14.83	13.74	14.27	14.69	12.49	10.61
NiO	0.15	0.11	0.29	0.16	0.08	0.10	0.14	0.18	0.15	0.27
Total	101.34	100.17	100.10	99.53	98.97	101.00	100.63	100.01	100.41	99.19
Ti	0.02	0.04	0.05	0.06	0.08	0.06	0.02	0.01	0.03	0.03
Al VI	4.26	4.05	4.74	5.09	5.61	5.77	6.12	0.83	6.89	8.34
V	0.02	0.06	0.01	0.03	0.02	0.03	0.03	0.01	0.02	0.02
Cr	11.10	11.28	10.63	10.42	9.79	9.65	9.22	1.11	8.46	7.03
Fe^{3+}	0.54	0.52	0.48	0.34	0.42	0.43	0.58	0.04	0.55	0.53
Mg	4.94	4.10	4.78	5.05	4.94	5.18	5.08	0.62	5.51	5.90
Mn	0.06	0.00	0.03	0.00	0.00	0.05	0.00	0.01	0.00	0.03
Fe^{2+}	2.99	3.90	3.22	2.99	3.12	2.80	2.92	0.38	2.51	2.08
Ni	0.03	0.02	0.06	0.03	0.02	0.02	0.03	0.00	0.03	0.05
#Cr	0.72	0.74	0.69	0.67	0.64	0.63	0.60	0.57	0.55	0.46
#Mg	0.62	0.51	0.60	0.63	0.61	0.65	0.63	0.62	0.69	0.74

bdl: below detection limit.

Pt, Pd and Ni, Cr_2O_3 for Cr, FeS_2 for Fe and S, Cu_2S for Cu, and GaAs for As. In this second routine, the X-ray lines measured were $K\alpha$ for S, Fe, Ni and Cr; $L\alpha$ for Ru, Rh, Pd, Os, Ir and Pt; and $L\beta$ for As. The following interferences were corrected online: $IrL\alpha \rightarrow CuK\alpha$, $RuL\beta \rightarrow RhL\alpha$, $CuK\beta \rightarrow OsL\alpha$. Because of the small size of the particles, raw data for PGM and BMM showed moderate Cr concentrations. These raw data were corrected according to the procedure described in detail by Augé (1988) and González-Jiménez et al. (2009b). At least two analyses were performed on each large PGM to check for homogeneity. Since laurite contain some amounts of Pt, Rh, Ni and Fe (Cabri, 2002) all these elements were also considered in the calculation of the structural formulae. Results of analyses of chromian spinel, silicates and PGM are given in Tables 1–5.

Four new chromitite samples were analyzed for all platinum-group elements (PGE) by Genalysis Laboratory Services Pty Ltd. at Maddington (Western Australia). In this laboratory, PGE were analyzed by ICP-MS after nickel sulfide fire-assay collection. Detection limits were 1 ppb for Rh, and 2 ppb for Os, Ir, Ru, Pt and Pd. Results are give in Table 4.

5. Chemistry of chromian spinel and silicates

About 500 electron microprobe analyses were carried out on chromian spinel and silicates from polished sections from chromitite as well as from the enclosing dunite and host harzburgite. Representative analyses of chromian spinel and silicates are given in Tables 1–3.

Table 2
Representative electron-microprobe analyses of accessory chromian spinel from dunite and harzburgite enclosing chromitites of the Sagua de Tánamo district. Dun: accessory chromian spinel in dunite, Hz: accessory chromian spinel in harzburgite.

	High-Cr chromitites					High-Al chromitites				
Sample	A-4	G-3A-P2	SI-101-P2	SI-103	A-2	C-5	C-5	NV	C	C2
	Dun	Dun	Dun	Hz	Hz	Dun	Dun	Dun	Hz	Hz
TiO_2	0.12	0.19	0.13	0.03	0.04	0.18	0.18	0.18	0.13	0.14
Al_2O_3	17.31	16.18	9.62	27.27	36.08	19.90	18.95	17.95	17.55	18.60
V_2O_3	0.14	0.22	0.30	0.15	0.22	0.17	0.16	0.15	0.17	0.29
Cr_2O_3	48.93	50.77	56.18	38.84	30.77	41.54	42.76	45.51	50.35	49.43
Fe_2O_3	4.50	3.53	4.16	4.02	2.77	8.83	8.35	6.70	2.62	2.25
MgO	11.29	11.17	8.35	14.28	14.40	10.55	9.90	10.67	10.72	10.68
MnO	bdl	bdl	bdl	bdl	0.24	bdl	bdl	bdl	bdl	*bdl*
FeO	17.44	17.42	20.55	14.00	15.16	19.15	20.01	18.49	18.49	18.70
NiO	0.13	0.07	0.09	0.09	0.14	0.21	0.22	0.09	0.14	0.11
Total	100.02	99.73	99.64	98.83	99.79	100.86	100.70	100.00	100.36	100.19
Ti	0.02	0.04	0.03	0.01	0.01	0.03	0.03	0.03	0.03	0.03
Al VI	5.19	4.89	3.06	7.78	9.83	5.91	5.68	5.40	5.26	5.55
V	0.03	0.05	0.07	0.03	0.04	0.03	0.03	0.03	0.03	0.06
Cr	9.85	10.30	11.97	7.43	5.63	8.27	8.59	9.19	10.13	9.90
Fe^{3+}	0.86	0.68	0.84	0.73	0.48	1.67	1.60	1.29	0.50	0.43
Mg	4.28	4.27	3.36	5.15	4.96	3.96	3.75	4.06	4.06	4.03
Mn	0.00	0.00	0.00	0.00	0.05	0.00	0.00	0.00	0.00	0.00
Fe^{2+}	3.71	3.74	4.63	2.83	2.93	4.03	4.25	3.95	3.93	3.96
Ni	0.03	0.02	0.02	0.02	0.03	0.04	0.05	0.02	0.03	0.02
#Cr	0.65	0.68	0.80	0.49	0.36	0.58	0.60	0.63	0.66	0.64
#Mg	0.54	0.53	0.42	0.65	0.63	0.50	0.47	0.51	0.51	0.50

bdl: below detection limit.

Please cite this article as: González-Jiménez, J.M., et al., High-Cr and high-Al chromitites from the Sagua de Tánamo district, Mayarí-Cristal ophiolitic massif (eastern Cuba): Constraints on..., Lithos (2011), doi:10.1016/j.lithos.2011.01.016

Table 3
Microprobe analyses (wt.% and calculated cations) of primary silicates of the Sagua de Tánamo chromitites, host rocks and enclosed gabbros.

Sample	High-Cr Chromitites							
	Inclusions chromian spinel chromitite			Chromitite matrix		Harzburgite		Gabbro
	Ol	Cpx	Opx	Amph	Amph	Opx	Opx	Amph
SiO_2	41.37	52.54	55.65	47.30	46.44	56.19	55.93	56.36
TiO_2	0.00	0.09	0.01	0.65	0.70	0.02	0.00	0.03
Al_2O_3	0.02	2.64	2.51	8.98	10.19	2.70	2.73	1.56
V_2O_3	–	–	0.00	–	–	–	–	–
Cr_2O_3	0.47	0.96	0.70	2.58	2.84	0.72	0.72	0.16
Fe_2O_3	–	0.00	0.00	–	–	0.45	0.58	–
MgO	53.85	16.88	32.21	22.12	20.30	33.86	32.94	32.80
CaO	0.01	23.54	2.11	10.37	11.86	0.96	2.20	0.43
MnO	0.06	0.10	0.13	0.01	0.05	0.02	0.15	0.14
FeO	4.01	2.20	5.56	1.97	2.30	5.57	5.07	7.48
NiO	1.00	0.06	0.06	–	–	0.02	0.10	–
Na_2O	–	0.06	0.00	2.44	2.67	0.00	0.00	0.01
K_2O	–	0.01	0.00	0.16	0.08	0.00	0.01	0.02
H_2O	–	–	–	2.12	2.12	–	–	2.24
Total	100.79	99.08	98.94	98.69	99.55	100.51	100.43	101.21
Si	0.99	1.93	1.95	6.69	6.56	1.93	1.93	7.56
Ti	0.00	0.00	0.00	0.07	0.07	0.00	0.00	0.00
Al	0.00	0.11	0.10	1.50	1.70	0.11	0.11	0.25
V	–	0.00	0.00	–		–		
Cr	0.01	0.03	0.02	0.29	0.32	0.02	0.02	0.02
Fe^{3+}	–	0.00	0.00	–	–	0.01	0.02	
Mg	1.91	0.92	1.68	4.66	4.27	1.73	1.69	6.56
Ca	0.00	0.93	0.08	1.57	1.79	0.04	0.08	0.06
Mn	0.00	0.00	0.00	0.00	0.01	0.00	0.00	0.02
Fe^{2+}	0.08	0.07	0.16	0.23	0.27	0.16	0.15	0.84
Ni	0.02	0.00	0.00	–	–	0.00	0.00	–
Na	–	0.00	0.00	0.67	0.73	0.00	0.00	0.00
K	–	–	–	0.03	0.02	–		0.00
Total	3.01	4.00	3.99	15.70	15.73	4.00	4.00	15.31
Mg#	0.96	0.93	0.91	0.95	0.94	0.92	0.92	0.89

Sample	High-Al chromitites						
	Inclusion in chromian spinel chromitite	Chromitite matrix		Harzburgite		Gabbro	
	Amph	Amph	Amph	Opx	Opx	Amph	Amph
SiO_2	44.63	48.97	49.42	57.87	56.88	43.43	44.17
TiO_2	0.50	0.31	0.39	0.02	0.02	2.41	2.15
Al_2O_3	11.74	8.48	7.89	1.72	1.53	9.98	9.16
V_2O_3							
Cr_2O_3	2.95	2.15	1.89	0.59	0.58	0.11	0.10
Fe_2O_3				0.25	2.82		
MgO	19.61	20.98	21.50	35.03	35.69	12.44	13.08
CaO	12.21	12.07	12.43	0.62	0.69	11.16	11.19
MnO	0.07	0.04	0.00	0.16	0.16	0.21	0.22
FeO	2.23	4.82	4.23	5.60	3.26	14.74	14.50
NiO	0.18	0.15	0.18	0.11	0.10		
Na_2O	2.76	1.68	1.50	0.02	0.00	2.21	2.01
K_2O	0.07	0.09	0.07	0.01	0.00	0.10	0.09
H_2O	2.10					2.00	2.00
Total	99.05	99.73	99.50	101.98	101.72	98.79	98.66
Si	6.36	6.79	6.94	1.96	1.93	6.51	6.61
Ti	0.05	0.03	0,03	0.00	0.00	0.27	0.24
Al	1.97	1.39	1,28	0.07	0.06	1.76	1.61
V							
Cr	0.33	0.24	0,23	0.02	0.02	0.01	0.01
Fe^{3+}				0.01	0,07		
Mg	4.17	4.34	4.43	1.76	1.80	2.78	2.92
Ca	1.87	1.79	1.79	0.02	0.03	1.79	1.79
Mn	0.01	0.00	0.00	0.00	0.01	0.03	0.03
Fe^{2+}	0.27	0.56	0.38	0.16	0.09	1.85	1.81
Ni	0.02			0.00	0.00		
Na	0.76	0.45	0.41	0.00	0.00	0.64	0.58
K	0.01	0.02	0.01			0.02	0.02
Total	15.82	15.61	15.50	4.00	4.00	15.66	15.63
Mg#	0.94	0.89	0.92	0.92	0.95	0.60	0.62

5.1. Chromian spinel

The chemistry of chromian spinel in the Sagua de Tánamo chromitites show a wide spectrum from high-Al to high-Cr (Figs. 4 and 5). The Cr# [(Cr/Cr + Al) atomic ratio] varies from 0.45 to 0.74 (corresponding to 38–55 wt.% Cr_2O_3 and 13–31 wt.% Al_2O_3) and Mg# [$(Mg/Mg+Fe^{2+})$ atomic ratio] from 0.57 to 0.74. The TiO_2 content is below 0.5 wt.% but is higher in high-Cr chromites (0.1–0.3 wt.%) than

Please cite this article as: González-Jiménez, J.M., et al., High-Cr and high-Al chromitites from the Sagua de Tánamo district, Mayarí-Cristal ophiolitic massif (eastern Cuba): Constraints on..., Lithos (2011), doi:10.1016/j.lithos.2011.01.016

Table 4
Whole-rock PGE concentrations (ppb) in the Sagua de Tánamo chromitites. (*) Data from Proenza et al. (1999) and Gervilla et al. (2005).

		Os	Ir	Ru	Rh	Pt	Pd	Total	Pd/Ir	Average PGE	Average Cr#
	High-Cr chromitites										
Tres Amigos	Ta-1	904	612	1809	98	69	5	3497	0.01	3497	0.72
Guarina	G-1*	48	45	111	21	42	7	274	0.2	392	0.71
	G-2*	112	121	209	33	27	8	510	0.1		
Monte Bueno	MB-1*	146	204	356	53	29	5	793	0.02	793	0.69
Caridad	SI-100*	529	1015	1787	134	235	13	3713	0.01	1445	0.66
	SI-103*	245	362	609	52	129	5	1402	0.01		
	SI-2*	110	210	120	43	43	12	537	0.1		
	CAR 300	97	115	247	27	34	5	525	0.04		
	CAR 301	248	216	508	41	30	8	1051	0.04		
Tibera	Ti-O3*	40	46	85	10	11	6	198	0.13	198	0.64
Albertina	A-100*	69	51	126	6	3	4	259	0.1	259	0.63
	High-Al chromitites										
Negro Viejo	NV-100*	58	46	81	4	6	2	197	0.04	151	0.6
	NV-1*	17	19	55	5	5	5	105	0.3		
Demajagua	DEM-2	44	38	102	6	7	5	202	0.13	202	0.59
Cernícalo	C3*	58	32	114	10	4	6	224	0.2	224	0.55
Rupertina	RU-1*	3	3	5	1	5	2	19	0.7	50.15	0.48
	R-100*	15	16	31	4	10	6	82	0.4		

in high-Al ones (0.1–0.2 wt.%). The Fe_2O_3 content varies between 0.4 and 5 wt.%. Minor amounts of MnO (0.1–0.3 wt.%), V_2O_3 (0.1–0.4 wt.%), NiO (0.1–0.3 wt.%) and ZnO (< 0.2 wt.%) were also detected. Chromitite samples in contact with gabbros have the lowest Mg#; and in the case of high-Cr chromitites the lowest Mg# is linked with the lowest Cr# and the highest TiO_2 (0.3–0.5 wt.%) contents.

In high-Cr chromitites the chromian spinel of dunite has similar or slightly higher Cr# (0.57–0.8; mean 0.69) compared with the chromian spinel of the chromitite (Fig. 5). The chromian spinel of the harzburgite enclosing these high-Cr chromitites has even lower Cr# (0.4–0.5; mean 0.45) than the chromian spinel of chromitite and dunite (Fig. 5).

In high-Al chromitites, the chromian spinel of the adjacent dunite has similar or slightly higher Cr# (0.58–0.63; mean 0.5) than the chromian spinel of chromitite, but lower Cr# than the chromian spinel of the surrounding harzburgite (0.57–0.66; mean 0.59) (Fig. 5).

The trend of increasing Cr# in chromian spinel from the host harzburgite towards high-Cr chromitites is also accompanied by an increase in the TiO_2 content: nil to 0.1 wt.% (mean 0.05 wt.%) in chromian spinel of harzburgite, from 0.06 to 0.2 wt.% (mean 0.13 wt.%)

Table 5
Selected PGM analyses from chromitites of the Sagua de Tánamo district. Laurite: 1–5, irarsite–hollingworthite: 6–10, iridium: 11–12, Ru–Os–Ir–Fe–Ni–(Rh) alloy/oxides (?): 13–14.

	Os	Ir	Ru	Pt	Pd	Rh	Fe	Cr	Ni	Cu	Co	S	As	Total
Raw analyses (wt.%)														
1	33.44	4.49	29.97	bdl	bdl	0.29	0.70	1.91	0.05	bdl	bdl	31.06	bdl	101.91
2	10.81	4.76	47.19	bdl	bdl	0.30	0.56	1.66	0.11	0.08	0.01	33.74	bdl	99.22
3	17.56	4.84	41.71	bdl	bdl	0.31	0.57	1.54	0.03	0.05	0.02	34.03	bdl	100.66
4	16.65	6.57	40.4	bdl	bdl	1.06	0.65	1.89	0.13	0.04	bdl	34.32	bdl	101.71
5	20.94	6.11	38.46	bdl	bdl	0.13	0.50	1.04	0.02	0.05	0.03	32.94	0.31	100.53
6	2.62	46.15	10.62	0.04	bdl	2.24	0.69	1.91	0.11	bdl	bdl	15.77	19.73	99.88
7	2.66	36.60	4.21	10.53	0.07	7.12	0.41	1.06	0.10	bdl	0.03	12.31	26.13	101.23
8	3.14	35.41	4.86	10.84	0	5.58	0.36	0.84	0.06	bdl	0.04	12.34	26.05	99.52
9	1.37	45.96	1.63	4.40	0.02	7.28	0.34	0.95	0.09	bdl	0.01	12.22	25.28	99.55
10	1.18	57.78	2.10	bdl	bdl	1.04	0.32	0.98	0.03	bdl	0.01	12.84	22.41	98.69
11	28.00	62.30	0.42	2.91	bdl	0.75	0.98	2.49	0.10	0.06	bdl	0.07	bdl	98.08
12	28.99	65.45	0.52	2.94	0.06	0.71	1.09	2.50	0.04	0.02	0.05	0.03	bdl	102.4
13	22.01	12.61	49.39	0.08	bdl	0.56	1.41	2.53	1.12	0.06	0.02	0.03	bdl	89.82
14	17.73	11.67	45.08	bdl	bdl	1.19	8.38	2.13	3.48	0.12	0.03	0.02	bdl	89.83
Recalculated analyses (at.%)														
1	11.88	1.58	20.05	0.00	0.00	0.19	0.76	–	0.06	0.00	0.00	65.48	0.00	
2	3.52	1.53	28.88	0.00	0.00	0.18	0.61	–	0.12	0.08	0.01	65.08	0.00	
3	5.76	1.57	25.73	0.00	0.00	0.19	0.48	–	0.03	0.05	0.02	66.17	0.00	
4	5.42	2.12	24.76	0.00	0.00	0.64	0.59	–	0.14	0.04	0.00	66.3	0.00	
5	7.05	2.04	24.37	0.00	0.00	0.08	0.33	–	0.02	0.05	0.03	65.77	0.26	
6	1.20	20.89	9.14	0.02	0.00	1.89	0.98	–	0.16	0.00	0.00	42.79	22.92	
7	1.26	17.15	3.75	4.86	0.06	6.23	0.48	–	0.15	0.00	0.05	34.58	31.42	
8	1.50	16.79	4.38	5.07	0.00	4.94	0.38	–	0.09	0.00	0.06	35.08	31.70	
9	0.67	22.12	1.49	2.09	0.02	6.54	0.44	–	0.14	0.00	0.02	35.25	31.22	
10	0.59	28.83	1.99	0.00	0.00	0.97	0.47	–	0.05	0.00	0.02	38.4	28.69	
11	28.58	62.94	0.81	2.90	0.00	1.42	2.42	–	0.33	0.18	0.00	0.42	0.00	
12	28.44	63.54	0.96	2.81	0.11	1.29	2.34	–	0.13	0.06	0.16	0.17	0.00	
13	16.30	9.24	68.85	0.06	0.00	0.77	1.79	–	2.69	0.13	0.05	0.13	0.00	
14	13.62	8.87	65.16	0.00	0.00	1.69	1.56	–	8.66	0.28	0.07	0.09	0.00	

bdl: below detection limit.

Please cite this article as: González-Jiménez, J.M., et al., High-Cr and high-Al chromitites from the Sagua de Tánamo district, Mayarí-Cristal ophiolitic massif (eastern Cuba): Constraints on..., Lithos (2011), doi:10.1016/j.lithos.2011.01.016

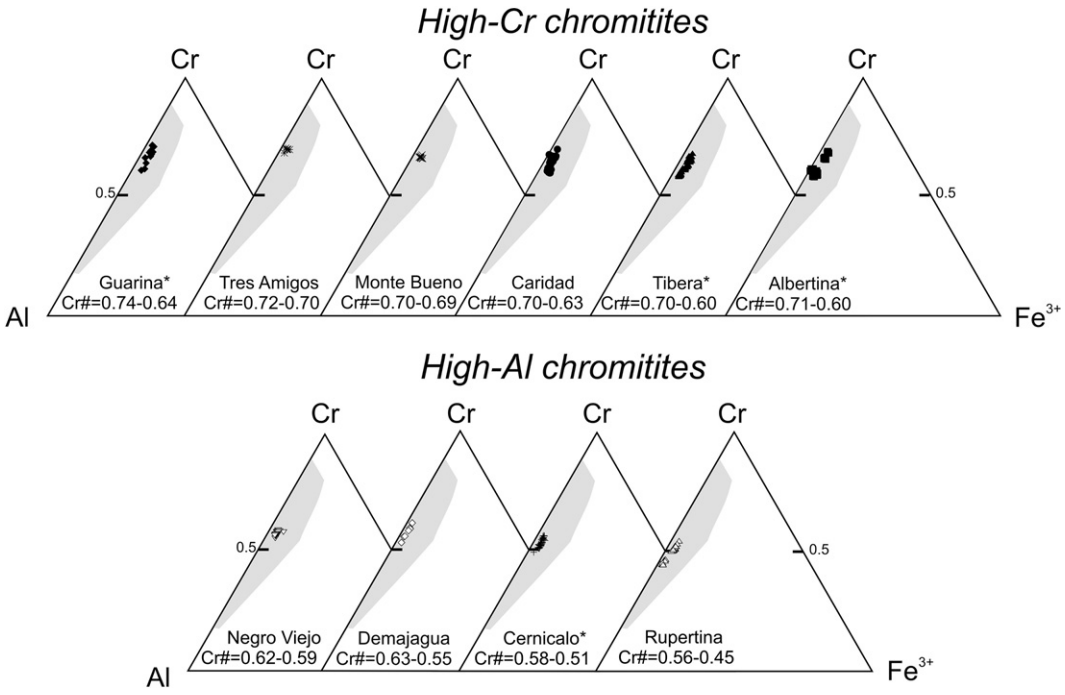

Fig. 4. Cr–Al–Fe^{3+} plots of chromian spinel in podiform high-Cr and high-Al chromitites. Ranges in Cr# are shown. Gray field shows the composition of podiform chromitites from ophiolites worldwide. (*) refers to chromitite hosting amphibole-bearing gabbros.

in chromian spinel of dunite, and between 0.1 and 0.3 wt.% (mean 0.19 wt.%) in the chromian spinel of chromitite (Fig. 6a).

In high-Al chromitite, TiO_2 contents in chromian spinel ranges between 0.1 and 0.24 wt.% in chromitite (mean 0.17 wt.% on average) and between 0.08 and 0.2 wt.% (mean 0.13 wt.%) in harzburgite, both are lower than the chromian spinel of dunite (0.14–0.21 wt.%; mean 0.19 wt.%) (Fig. 6b).

5.2. Silicates

5.2.1. Olivine

Unaltered olivine useable for electron-microprobe analyses has only been preserved as inclusions in the cores of chromian spinel grains in high-Cr chromitites. These olivines are forsterite (Mg# = 0.96), containing NiO (<1.59 wt.%), Cr_2O_3 (<0.69 wt.%) and MnO (<0.1 wt.%) (Table 3).

5.2.2. Pyroxenes

Pyroxenes have only been identified as inclusions in chromian spinel in Cr-rich chromitites. Clinopyroxene is diposide ($En_{47-48}Fs_{3-4}Wo_{48-50}$) with relatively high Mg# (0.93–0.96), which roughly correlates with Cr_2O_3 (0.9–1.5 wt.%) and TiO_2 (<0.1 wt.%) (Fig. 7). The Al_2O_3 content reaches 2.7 wt.% and Na_2O is lower than 0.11 wt.%. Orthopyroxene inclusions are enstatite ($En_{87-90}Fs_9Wo_{1-4}$; Mg# = 0.91), with minor contents of Cr_2O_3 (<0.7 wt.%), TiO_2 (0.01–0.04 wt.%) and Al_2O_3 (<2.5 wt.%) (Fig. 7)).

Orthopyroxene in harzburgite enclosing high-Cr chromitites has similar Mg# (0.91–0.92) and TiO_2 values (0.01–0.04 wt.%) but higher contents of Cr_2O_3 (0.7–0.8 wt.%) and Al_2O_3 (2.5–2.9 wt.%) than orthopyroxene inclusions in chromian spinel (Fig. 7). In contrast, orthopyroxene from harzburgite hosting high-Al chromitites is relatively more magnesian ($En_{89-90}Fs_{8-9}Wo_{1-2}$; Mg# 0.92–0.95) with similar contents of TiO_2 (<0.05 wt.%) and Al_2O_3 (1.5–2 wt.%) but the lowest Cr_2O_3 contents (0.3–0.68 wt.%) (Fig. 7).

5.2.3. Amphibole

Amphibole has only been analyzed as inclusions in chromian spinel in high-Al chromitites, and in chromian spinel grains from dunite hosting high-Cr-chromitites. The former is pargasite (Fig. 7) with high Mg# (0.94), and high contents of Cr_2O_3 (<2.9 wt.%) and Na_2O (<2.76 wt.%), as well as low TiO_2 (<0.5 wt.%) and K_2O (<0.1 wt.%). In contrast, amphibole included in chromian spinel from dunite is mainly edenite (Fig. 7) having similar Mg# (0.93–0.94) and higher values of Cr_2O_3 (<3.3 wt.%), Na_2O (<2.76 wt.%) and TiO_2 (<0.6 wt.%), and similar contents of K_2O (<0.1 wt.%).

Amphibole of the interstitial matrix of high-Cr chromitites is mainly edenite with high Mg# (0.93–0.96), and high contents of Cr_2O_3 (<3.3 wt.%), Na_2O (<3.05 wt.%), TiO_2 (<0.84 wt.%) and low K_2O (<0.2 wt.%)(Fig. 7). This is very similar to the amphibole found as inclusions in chromian spinel of the enclosing dunite, and significantly different from the amphibole of the gabbros embedded in the chromitite. Amphibole from the gabbros is slightly less magnesian (Mg# = 0.89) and poorer in Cr_2O_3 (<0.30 wt.%) and Na_2O (<2.5 wt.%), with slightly higher TiO_2 (<0.88 wt.%) than amphibole of the interstitial matrix of the chromitite, but identical K_2O (<0.2 wt.%).

Amphibole in the interstitial matrix of high-Al chromitite is also edenitic. Compared to the interstitial amphibole of high-Cr chromitite, it has slightly lower Mg# (0.88–0.92) and Cr_2O_3 (<2.2 wt.%), Na_2O (<1.68 wt.%) and TiO_2 (<0.4 wt.%) and K_2O (<0.1 wt.%) contents (Fig. 7). Amphibole from gabbros included in high-Al chromitite show the lowest Mg# (0.6–0.8) among the analyzed amphiboles, Cr_2O_3 contents up to 0.78 wt.%, and the highest values of TiO_2 (<2.5 wt.%) and Al_2O_3 (7.6–12.2 wt.%) (Fig. 7). The contents of Na_2O (1.3–2.22 wt.%) and K_2O (0.04–0.11 wt.%) are similar to the other amphiboles.

6. Platinum-group elements: abundance and distribution

Total PGE abundances of the chromitites are low (below 800 ppb on average) although PGE distribution is not homogeneous within single chromitite bodies (e.g., between 525 and 3713 ppb in the high-Cr chromitite of Caridad; Table 4). The chondrite-normalized PGE patterns of the chromitites of Sagua de Tánamo are typical of ophiolitic chromitites elsewhere. They display a steep negative slope from the Ir-group (IPGE: Os, Ir and Ru) to the Pt-group (PPGE: Pt, Pd

Please cite this article as: González-Jiménez, J.M., et al., High-Cr and high-Al chromitites from the Sagua de Tánamo district, Mayarí-Cristal ophiolitic massif (eastern Cuba): Constraints on..., Lithos (2011), doi:10.1016/j.lithos.2011.01.016

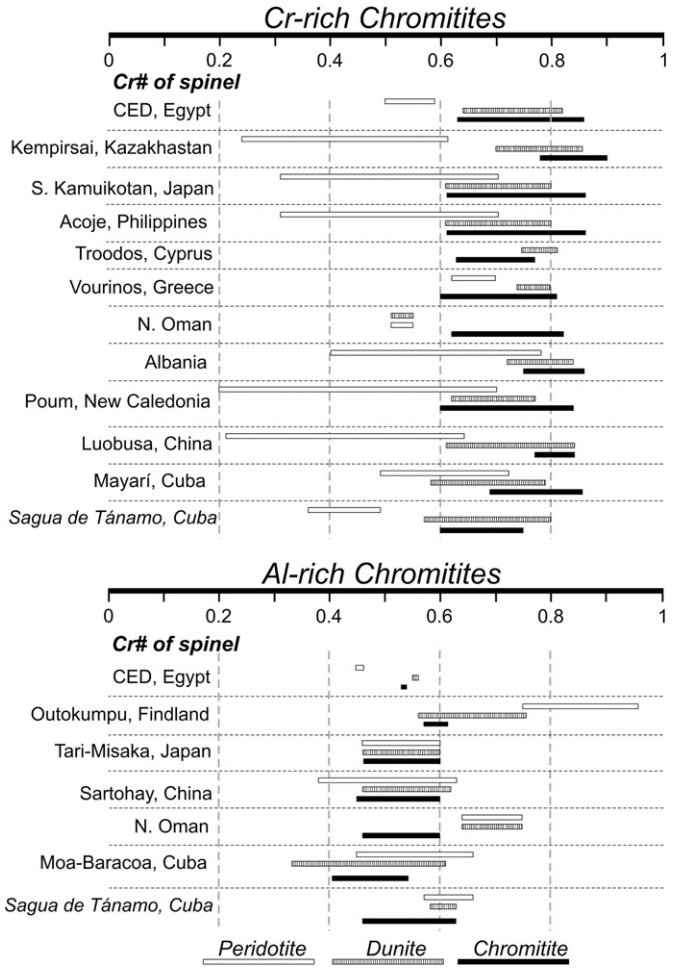

Fig. 5. Comparison of Cr# in chromian spinel from chromitites and enclosing host rocks in the Sagua de Tánamo district, and in podiform high-Cr and high-Al chromitites of some ophiolitic complexes. Data sources for high-Cr chromitites: CED, Egypt (Ahmed et al., 2001); Kempirsai, Kazakhastan (Melcher et al., 1994, 1997, 1999); S. Kamuikotan, Japan (Arai, 1997); Acoje, Philippines (Rammlmair et al., 1987); Troodos, Cyprus (Augé and Johan, 1988; McElduff and Stumpfl, 1991); Vourinos, Greece, (Economou, 1983; Economou et al., 1986; Economou-Eliopoulos, 1996 and Konstantopoulou and Economou-Eliopoulos, 1991); N. Oman (Ahmed and Arai, 2002; Rollinson, 2005); Albania (Kocks et al., 2007); Poum, New Caledonia (Leblanc, 1995); Luobusa, China (Zhou and Bai, 1992; Zhou and Robinson, 1994; Peng et al., 1995; Zhou et al., 1996); Mayarí, Cuba (Proenza et al., 1999; Gervilla et al., 2005). Data sources for high-Al chromitites: CED, Egypt , Outokumpu, Findland, and Tari-Misaka, Japan (Arai, 1997 in Ahmed et al., 2001); Sartohay, China (Zhou and Bai, 1992; Zhou and Robinson, 1994; Peng et al., 1995; Zhou et al., 1996); Moa-Baracoa, Cuba (Proenza et al., 1999; Gervilla et al., 2005).

and Rh) with very low Pt–Pd contents, they consequently exhibit very low Pd/Ir ratios (0.01–0.7) (Fig. 8a and b).

PGE contents in high-Cr chromitites vary from 198 to 3713 ppb (mean 1956 ppb), but range from 18 to 224 ppb (mean 121) in high-Al chromitites (Table 4). The PGE-normalized patterns in high-Cr chromitites have steeper slopes (mean Pd/Ir = 0.1) than those in high-Al chromitites (mean Pd/Ir = 0.4). As a consequence bulk PGE contents are positively correlated with the Cr content of chromite in the chromitite, and negatively correlated with Pd/Ir (Fig. 8c and Table 4).

7. Platinum-group elements and base-metal minerals

180 PGM grains were indentified *in-situ* in the investigated chromitites. The PGM are distributed heterogeneously; they were only found in samples from five of the ten investigated chromitite bodies. The PGM are rare in high-Al chromitites (only three grains were found in Negro Viejo), whereas they are more ubiquitous in high-Cr chromitites (110 grains in Caridad, 46 in Monte Bueno, 20 in Tres Amigos, 1 in Albertina, and none in Tibera and Guarina).

Most of the PGM grains occur as inclusions in chromian spinel (134 in unaltered cores and 2 in ferrian chromite rims), although 44 PGM grains were found along fractures or in the altered silicate matrix between grains of chromian spinel. As a general rule, PGM in the unaltered cores of chromian spinel are euhedral (Figs. 9a–d) whereas PGM in ferrian chromite, fractures or the serpentinized silicate matrix tend to be subhedral or irregular (Fig. 9e-i). Some grains located in fractures or in the silicate matrix show inner porous textures (Figs. 9g and h). The size of PGM is usually less than 25 μm, although some grains in fractures or in the silicate matrix may be up to 60 μm across.

About 60% of identified PGM are members of the laurite (RuS_2)-erlichmanite (OsS_2) solid solution series, 15% are members of the irarsite (IrAsS)-hollingworthite (RhAsS) solid solution series and 13% are Ru–Os–Ir–Fe–Ni–(Rh) alloy/oxides. Other less abundant minerals are Ir-rich alloys (8%), cuproiridsite (2%), an unidentified Ir-sulfide (1%) and an undescribed mineral close to RhNiAs (1%).

Minerals of the laurite–erlichmanite series occur as single grains or associated with other PGM, base metal sulfides (millerite or pentlandite) or silicates (Fig. 9a and b). The composition ranges between Os-rich laurite $[(Ru_{0.56}Os_{0.29}Ir_{0.11}Ni_{0.03}Cu_{0.02})_1\ S_2]$ and Os-poor laurite $[(Ru_{0.91}Os_{0.06}\ Ir_{0.04}Fe_{0.01})_{1.02}S_{1.98}]$ (Fig. 10a), with Os and Ir contents varying from 6.4 to 33.7 wt.% (mean 21 wt.%) and 2–9 wt.% (mean 5.5 wt.%), respectively. Arsenic is below 2 wt.% (Table 5). Erlichmanite was not analyzed quantitatively because of its small grain size (<2 μm). Some laurite grains found inside unaltered chromian spinel cores display zoning in Os content, and in a few cases drop-like to subhedral inclusions of Ni–Cu–Fe sulfides (mainly millerite, chalcocite and pentlandite) occur aligned in bands defining zoning (González-Jiménez et al., 2009b). Laurite grains in ferrian chromite alteration rims or fractures filled by secondary silicates show irregular outlines (Fig. 9e) and systematically lower S and Os.

Sulpharsenides of the irarsite-hollingworthite solid solution series in the unaltered cores of chromian spinel occur as single (sometimes zoned; Fig. 9c) or composite grains with laurite. In the matrix these sulpharsenide are associated with grains of partially desulphurized laurite or Ru–Os–Ir–Fe–Ni–(Rh) alloy/oxide (?) located in fractures. The composition of the sulpharsenides varies from Ru-rich irarsite $[(Ir_{0.87}Ru_{0.06}Rh_{0.03}Os_{0.02}Fe_{0.01})_{0.98}As_{0.86}S_{1.15}]$ to Ir-rich hollingworthite $[(Rh_{0.52}Ir_{0.30}Ru_{0.20}Pt_{0.01}Os_{0.01})_{1.05}As_{0.73}S_{1.22}]$ (Fig. 10b and Table 5). Irarsite grains in the unaltered cores of chromian spinel show higher Ru and Os concentrations (up to 10.9 and 16 wt.%, respectively) than those in altered zones (up to 3.5 and 1.79 wt.%, respectively) (Fig. 10b). However, grains located in fractures are richer in Pt (up to 11 wt.%) than those in unaltered cores of chromian spinel.

A set of distinctive grains consisting of IPGE with Fe, Ni and Rh were recognized in the fractures and in the silicate matrix (Fig. 9g and h). These grains show lower brightness in reflected light than the other PGM and have a spongy texture. They yield lower analytical totals than typical alloys enclosed in unaltered cores of chromian spinel (Table 5). Grains with similar features have been described in the literature as PGE oxides (e.g., Garuti et al., 1997; Uysal et al., 2009b). However, recent results by Hattori et al. (2010) suggest that these minerals cannot be PGE oxides but, are mixtures between PGE in the metallic state and Fe-oxides and/or hydroxides. In the absence of data on the crystal-chemistry of these grains, we will refer to them as PGE alloy/oxide (?). The Ru, Os and Ir atomic proportions of these PGE alloy/oxides (?) approach those of laurite from altered zones and strongly differ from the Ir-dominated alloys (Fig. 10c). Grains in fractures are richer in PGE (50–62 wt.% Ru, 17–25 wt.% Os, 8–13 wt.% Ir and up to 1.4 wt.% Rh) and poorer in base-metals (1.1–11 wt.% Fe and <0.4 wt.% Ni) than those located in the silicate matrix (34–62 wt.% Ru, 9.5–19 wt.% Os, 6.7–18.9 wt.% Ir; and 14.8–34 wt.% Fe and 1.1–2.6 wt.% Ni) (Fig. 10c and d). Some of the analyzed grains retains some As and S (up to 2.30 and 0.06 wt.%, respectively).

Please cite this article as: González-Jiménez, J.M., et al., High-Cr and high-Al chromitites from the Sagua de Tánamo district, Mayarí-Cristal ophiolitic massif (eastern Cuba): Constraints on..., Lithos (2011), doi:10.1016/j.lithos.2011.01.016

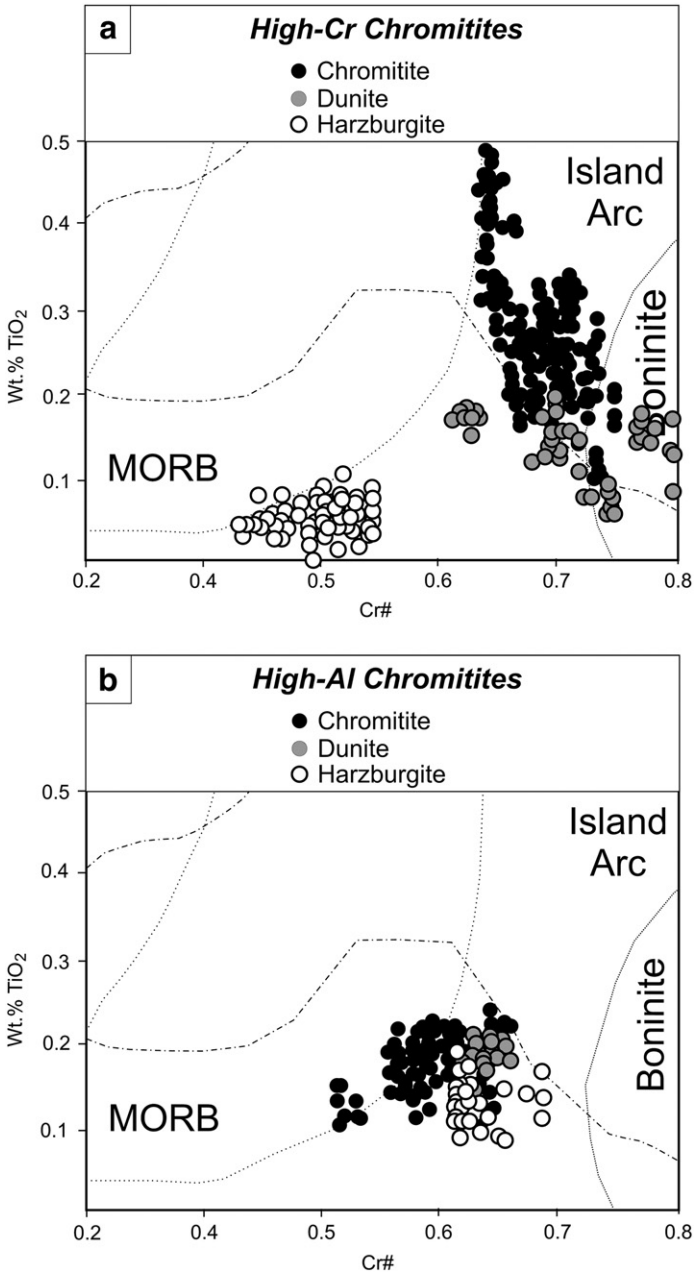

Fig. 6. Relation between TiO_2 and Cr# of chromian spinel in podiform high-Cr and high-Al chromitites and enclosing host rocks. Fields of chromian spinel in lavas of different geochemical affinities and tectonic settings are shown for comparison (Arai, 1992).

Iridium ($Ir_{0.66}Os_{0.33}Ru_{0.01}$) forms composite grains with laurite, or the Ir-sulfide (Fig. 9d).

Cuproiridsite [$Cu_{0.92}Ni_{0.17}Fe_{0.04})_{1.13}(Ir_{1.28}Pt_{0.29}Rh_{0.01}Rh_{0.01})_{1.85}S_{4.02}$] occurs only as composite inclusions with laurite and/or silicates in unaltered cores of chromian spinel grains.

The sulfide containing Ir is too small to allow proper quantitative analysis. Semi-quantitative analyses suggest that it could be kashinite (Ir_2S_3) (?). It occurs associated with laurite or iridium in composite aggregates (Fig. 9d).

The unknown RhNiAs phase occurs as an alteration rim on hollingworthite or forms a composite grain with a Ru–Os–Ir–Fe–Ni alloy/oxide (?) in the serpentinized silicate matrix. Its average structural formula is close to $Rh_{0.95}Ni_{1.04}As_{1.02}$. This undescribed mineral was also reported from the Mayarí-Baracoa Ophiolitic Belt chromitites by Gervilla et al. (2005).

In addition to PGM, chromitites usually exhibit a great variety of inclusions of base-metal minerals (BMM). Millerite (NiS) and heazlewoodite (Ni_3S_2) are the most abundant, followed by Cu–Fe sulfides [chalcopyrite ($CuFeS_2$), bornite (Cu_5FeS_4) and chalcocite (Cu_2S)], pentlandite [$(Ni,Fe)_9S_8$], awaruite (Ni_3Fe), native Cu and orcelite ($Ni_{5-x}As$). Millerite, pentlandite, chalcopyrite, bornite and chalcocite occur as inclusions in unaltered chromite. In contrast, heazlewoodite, awaruite, chalcocite and native Cu occur as replacement of pentlandite or chalcopyrite and bornite, respectively, in the altered zones, suggesting their secondary origin. Orcelite was only found in the altered silicate matrix.

8. Discussion

8.1. Constrains on the compositions of the parental melt of chromitite

Valuable information on the geochemical signature of the chromite parental magmas and the tectonic setting of their genesis can be obtained by studying the composition of unaltered cores of

Please cite this article as: González-Jiménez, J.M., et al., High-Cr and high-Al chromitites from the Sagua de Tánamo district, Mayarí-Cristal ophiolitic massif (eastern Cuba): Constraints on..., Lithos (2011), doi:10.1016/j.lithos.2011.01.016

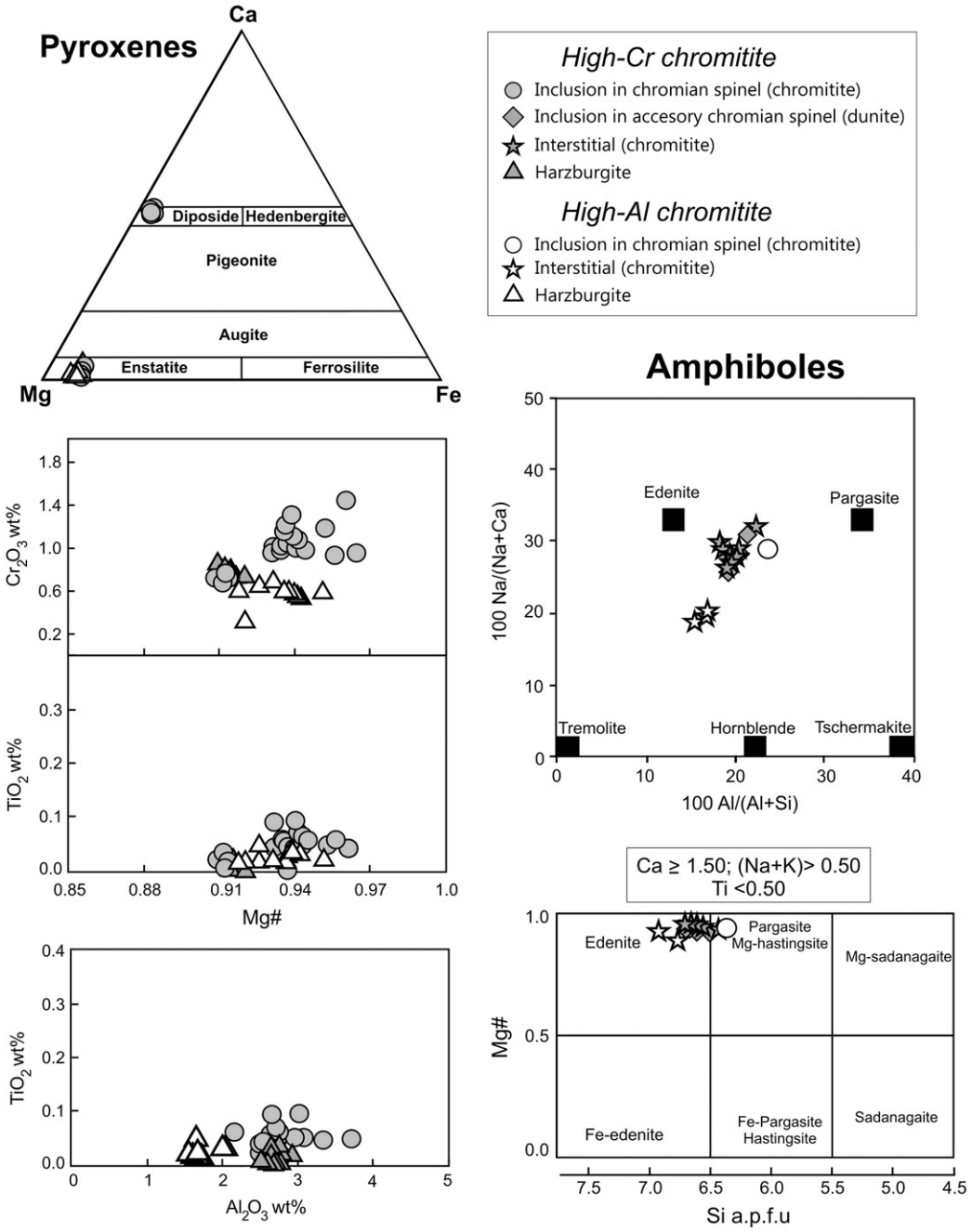

Fig. 7. Compositional variations of silicates in the high-Cr and high-Al chromitites of the Sagua de Tánamo, compared with host harzburgite and dunite.

chromian spinel. However reactions between Cr–Al spinel and silicates during cooling may produce a significant exchange of elements. Therefore, interpretations of the compositional variation in chromian spinel of the Sagua de Tánamo chromitites in terms of primary magmatic processes first require an assessment of the potential effect of subsolidus element re-distribution.

The elevated Mg# and high Cr_2O_3 contents of olivine and clinopyroxene inclusions in chromian spinel from high-Cr chromitites indicate that these silicates may have been equilibrated with chromian spinel during cooling. However, orthopyroxene inclusions in chromian spinel of chromitite and harzburgite are identical in composition. Amphibole inclusions in chromian spinel and in the silicate matrix of both types of chromitites also show similar chemistry. These observations suggest that, although subsolidus re-equilibration may have occurred, the primary magmatic compositional trends of chromian spinel (and silicates) were not substantially disturbed since the magmatic stage. Furthermore, as the extent of the component exchange is strongly dependent on chromite/silicate ratio, the fact that almost all the chromitite bodies mainly consist of monomineralic chromian spinel (i.e. massive-textured ore), with only very minor amounts of silicates present as inclusions, suggests that the composition of chromian spinel in most of the studied chromitite samples has not changed significantly from its high-temperature magmatic composition.

The chromian spinel of chromitites associated with gabbros has the lowest Mg#, and in the case of high-Cr chromitites the lowest Cr# and highest TiO_2 values. The lower Mg#, Cr_2O_3 and higher TiO_2 and Al_2O_3 in amphibole of the enclosed gabbros relative to amphibole in the chromitites suggest that the parental melt of the chromitites could partially assimilate pre-existing gabbros, becoming richer in Al, Ti and H_2O, and producing more Al- and Ti-rich chromian spinel and precipitating abundant interstitial amphibole (e.g., Leblanc and Violette,

Please cite this article as: González-Jiménez, J.M., et al., High-Cr and high-Al chromitites from the Sagua de Tánamo district, Mayarí-Cristal ophiolitic massif (eastern Cuba): Constraints on..., Lithos (2011), doi:10.1016/j.lithos.2011.01.016

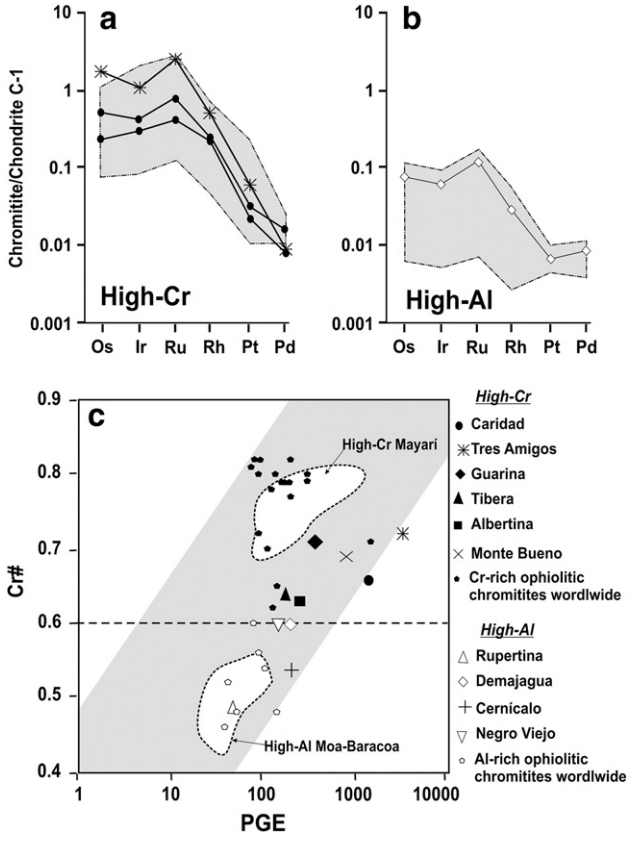

Fig. 8. Chondrite (Naldrett and Duke, 1980) normalized PGE patterns of high-Cr (a) and high-Al chromitites (b) from the Sagua de Tánamo district. Gray fields are compilation of data from Proenza et al. (1999) and Gervilla et al. (2005). (c) Cr# versus bulk PGE content in Cr-rich and Al-rich chromitites of the Sagua de Tánamo district and other podiform ophiolite chromitites. Only analyses of massive chromitites (from not significantly altered ophiolite complexes) are plotted. Data sources for high-Cr chromitites: Mayarí, Eastern Cuba (Proenza et al., 1999; Gervilla et al., 2005), Greek ophiolites (Vourinos, Kissavos, Pindos, Thessaly, Vermio, Veria, Edessa; Konstantopoulou and Economou-Eliopoulos, 1991; Economou-Eliopoulos, 1996), Serbian ophiolites (Radusa, Brecovitsa, Veluce; Economou-Eliopoulos, 1996), Oman (Ahmed and Arai, 2002), Luobusa (Zhou et al., 1996). Data sources for high-Al chromitites: Moa-Baracoa (Proenza et al., 1999; Gervilla et al., 2005), Greek ophiolites (Othrys, Kissavos, Rodiani, Pindos; Economou-Eliopoulos, 1996), Oman (Ahmed and Arai, 2002).

1983; Bédard and Hébert, 1998; Proenza et al., 1999). The observation that such compositions of spinel, and abundant interstitial amphibole, were only observed in proximity to the gabbros and at the scale of chromitite hand samples, lead us to suggest that this mechanism probably was restricted to within a few centimeters from the contact with gabbros.

Accepting the above arguments, only compositions from massive chromitites, not associated with gabbros, have been used to estimate the compositions of the parental melts in equilibrium with the Sagua de Tánamo chromitites.

Experimental studies of spinel-liquid equilibrium at 1 bar (Maurel and Maurel, 1982) indicate that the Al_2O_3 content of the melt from which chromian spinel crystallized can be determined using the following equation: $(Al_2O_3)_{spinel} = 0.035(Al_2O_3)^{2.42}$. This formulation assumes that Al_2O_3 in spinel is only a function of Al_2O_3 in the melt. Kamenetsky et al. (2001) also have shown, using melt inclusions in chromian spinel from volcanic rocks, that there is a linear relationship between the Al_2O_3 and TiO_2 contents of chromian spinel and the melt from which it crystallized. The contents of Al_2O_3 of the melts in equilibrium with spinel estimated by both methods correspond closely (Mondal et al., 2006 and Mukherjee et al., 2010). The TiO_2 content of the melt can be determined from the melt-TiO_2 versus spinel-TiO_2 regression lines developed by Zaccarini et al. (in press) using the data of Kamenetsky et al. (2001). The FeO/MgO ratio of the melt can also be computed for nearly monomineralic chromitite (i.e., "massive chromitites") using the formula proposed by Maurel and Maurel (1982): $Ln(FeO/MgO)_{spinel} = 0.47 - 1.07Al\#_{spinel} + 0.64Fe^{3+}\#_{spinel} + Ln(FeO/MgO)_{melt}$ with FeO and MgO in wt.%, $Al\# = Al/(Cr + Al + Fe^{3+})$ and $Fe^{3+}\# = Fe^{3+}/(Cr + Al + Fe^{3+})$.

Applying the approach of Kamenetsky et al. (2001), and using the regression lines obtained by Zaccarini et al. (in press) we have calculated the Al_2O_3 and TiO_2 contents of the melt in equilibrium with massive chromitites of the Sagua de Tánamo district. The FeO/MgO ratio of the melt has been calculated using the formula of Maurel and Maurel (1982). Results are shown in Table 6 and represented graphically in Fig. 11. The melts that produced the chromian spinel of the Sagua de Tánamo high-Cr chromitites contained 13–14 wt.% Al_2O_3 and relatively high TiO_2 (0.2–0.4 wt.%), with FeO/MgO ratios varying between 0.9 and 1.5. In contrast, the melts that produced the chromian spinel of the high-Al chromitites may have had higher Al_2O_3 (15–16 wt.%) and TiO_2 (0.3–0.5 wt.%) contents, and FeO/MgO ratios ranging between 0.9 and 1.1 (Table 6). The compositions of the melts parental to the chromian spinel of the Sagua de Tánamo high-Cr chromitites resemble the boninites of Bonin Island, Japan (e.g., Hicky and Frey, 1982; Crawford et al., 1989). Similar melts of boninitic affinity but with lower Al_2O_3, TiO_2 and FeO/MgO have been suggested to be responsible for the formation of high-Cr chromitites from many localites. Examples include Kempirsai in Kazakhstan (Melcher et al., 1997), Oman (Rollinson, 2008), Muğla in Turkey (Uysal et al., 2009a), Rutland Island in the Bay of Bengal (Ghosh et al., 2009), and Santa Elena in Costa Rica (Zaccarini et al., in press).

In contrast, chromian spinel of the Sagua de Tánamo high-Al chromitites may have crystallized from melts broadly similar to normal MORB (Al_2O_3 content ~16 wt.%), but with lower TiO_2 values and FeO/MgO which suggest an affinity to back-arc basin basalts (e.g., Dick and Bullen, 1984; Wilson, 1989; Mudholkar and Paropkari, 1999). The suggested parental melts of the Sagua de Tánamo high-Al chromitites are identical to those reported by Melcher et al. (1997) as responsible for the formation of the high-Al chromitites of the Batamshink ore field in Kazakhstan. They are somewhat different (i.e., higher values of Al_2O_3, TiO_2 and FeO/MgO) from those of N-MORB considered as the parental melt for the high-Al chromitites of Oman (Rollinson, 2008) and Muğla in Turkey (Uysal et al., 2009a).

8.2. Genesis of chromitite

The mechanism of chromian spinel crystallization to form large volumes of chromitites in ophiolitic mantle rocks is still matter of debate. Since the early 1980s diverse models have been proposed: (1) cotectic crystallization of chromite + olivine followed by mechanical separation within open conduits in the upper mantle (Lago et al., 1982; Leblanc and Ceuleneer, 1992), (2) changes in fO_2 or degree of polymerization in the melt (McElduff and Stumpfl, 1991; Melcher et al., 1997; Proenza et al., 1999; Edwards et al., 2000), (3) assimilation of pre-existing mafic rocks by peridotitic intrusions (Bédard and Hébert, 1998), (4) accumulation of chromite into a water-rich fraction segregated from a water-rich and chromite–olivine saturated basaltic melt (Matveev and Ballhaus, 2002), (5) mixing of variably differentiated (more or less SiO_2-rich) basaltic melts within dunitic channels after melt–peridotite reactions (Arai and Yurimoto, 1994; Zhou et al., 1996, 1998; Ballhaus, 1998).

Our findings support a model for chromitite formation by melt–rock reaction combined with melt–melt interaction. In this model ascending mantle melts react with harzburgite, resulting in the dissolution of (ortho)pyroxenes and the precipitation of olivine; this produces the dunite wall rocks and shifts the composition of the migrating melt towards higher Si and Cr. The precipitation of olivine focused along discrete zones and/or discontinuities of the host rock may form flow melt channels (Lago et al., 1982) in which batches of primitive melt fed into the conduit may interact with pools of relatively more evolved

Please cite this article as: González-Jiménez, J.M., et al., High-Cr and high-Al chromitites from the Sagua de Tánamo district, Mayarí-Cristal ophiolitic massif (eastern Cuba): Constraints on..., Lithos (2011), doi:10.1016/j.lithos.2011.01.016

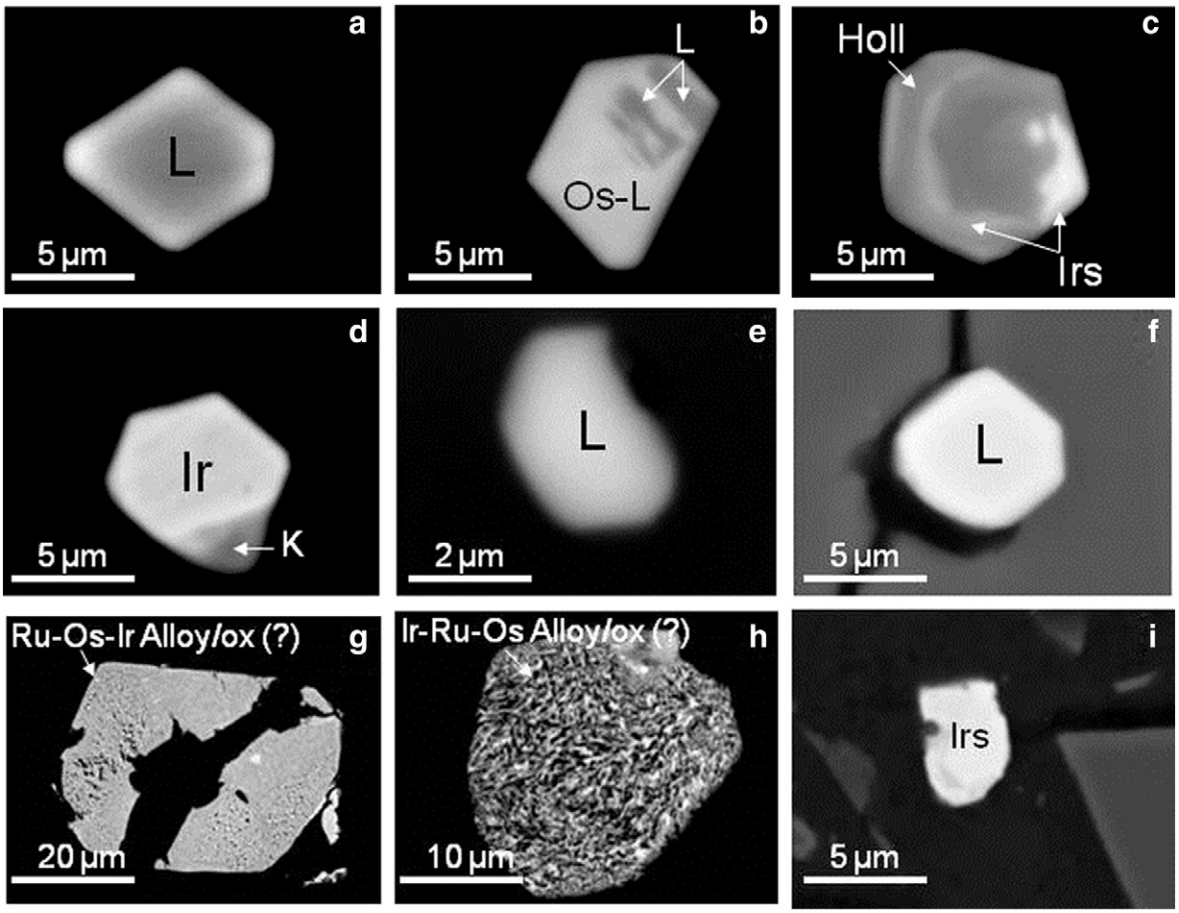

Fig. 9. Backscattered-electron images of platinum-group minerals in the Sagua de Tánamo chromitites. (a–d) Grains enclosed in unaltered cores of chromian spinel, (e) grain in ferrian chromite alteration rim, (f–h) minerals in fractures, (i) grain in interstitial silicate matrix. Keys: L: laurite, Os-L: Os-rich laurite, Irs: irarsite, Holl: hollingworthite, Ir: iridum, K: iridium sulfide (probably kashinite), Ru–Os–Ir Alloy/ox (?): Ru–Os–Ir alloy/oxide (?), Ir–Ru–Os Alloy/ox (?): Ir–Ru–Os alloy/oxide (?).

melt (Arai and Yurimoto, 1994; Zhou et al., 1996). The mixing/mingling of melts with variable degrees of fractionation may produce hybrid melts within the spinel + liquid region of the olivine–silica–spinel system, promoting the crystallization of chromian spinel alone (Irvine, 1977; Ballhaus, 1998). Thus, a continuous supply of melt favors both the melt–rock reaction and the replenishment of the conduit, enabling the protracted formation of hybrid melts, and therefore the formation of chromitites of variable size.

Experimental data by Ballhaus (1998) and Matveev and Ballhaus (2002) support this model and attest to the role of the water in the melt for the effective concentration of chromian spinel. The idea that melt–rock reactions play an important role in the formation of the chromitites is supported by the dunite cocoons that usually surround chromitites, which are interpreted to be partly replacive in origin because of the dissolution of (ortho)pyroxene from the harzburgite wall-rock (e.g., Arai and Yurimoto, 1994; Zhou et al., 1996) and partly cumulative after olivine precipitation (e.g., Matsumoto and Arai, 2001; Pagé and Barnes, 2009).

In the Sagua de Tánamo high-Cr chromitites, the relations between Cr# and TiO_2 suggests that the chromian spinel of both chromitite and dunite precipitated from low-Ti island arc tholeiite (IAT) with boninitic affinity, whereas the chromian spinel of the host harzburgite has a composition that roughly coincides with those of MORB (or back-arc basin basalts) (Fig. 5). This observation indicates that chromitite and dunite crystallized in equilibrium from a common parental melt that was different from those extracted during formation of the harzburgite. This is consistent with the compositions of chromian spinel (Cr# ≥ 0.8) from the extrusive boninitic lavas (i.e., Téneme formation) spatially associated with the peridotites (Proenza et al., 2006). This confirms that chromitite (and dunite) were produced by migrating IAT melts of boninitic affinity that percolated through the Sagua de Tánamo mantle before erupting as Cr-rich boninitic flows. In Fig. 6a the composition of spinel from the chromitite (and dunite) plots between the fields of IAT and boninite. This may imply that the migrating melts with boninitic affinity have had their composition modified by the reaction with the harzburgite wall-rocks, moving toward a more evolved boninite-like melt (e.g., Zhou et al., 1996). This would explain the relative Ti character (~0.4 wt.% TiO_2) of the parental melts in equilibrium with high-Cr chromitites (e.g., Kelemen, 1990; Mondal et al., 2006; Pagé and Barnes, 2009). Moreover, the predominantly anhedral morphology of chromian spinel in both the harzburgite wall-rocks and the dunite envelopes provides further evidence that the chromitite–dunite assemblage was generated by extensive reaction between harzburgite and migrating mantle melts (e.g., Matsumoto and Arai, 2001). This may have occurred when melt flow focused along fractures or sub-vertically oriented channels formed at shallower depths in the upper mantle (<20 km) (Quick, 1981; Quick and Gergory, 1995; Kelemen et al., 1999), as shown by the dike-like nature (i.e., discordant) of some chromitite–dunite assemblages with respect to the surrounding peridotites (e.g., Arai and Yurimoto, 1995; Zhou et al., 1996; Matsumoto and Arai, 2001).

The positive correlation between the Cr_2O_3 content of the spinel in a chromitite and thickness of its dunite envelope suggests that with increasing melt volume, the extent of melt–rock reaction (i.e., permeation of melts towards wall harzburgite) may have increased (Fig. 12a). The net effect of this process was the removal of large proportions of Cr-rich orthopyroxene to produce more Cr-rich melts and, the production of abundant olivine (Fig. 12a). In such a scenario,

Please cite this article as: González-Jiménez, J.M., et al., High-Cr and high-Al chromitites from the Sagua de Tánamo district, Mayarí-Cristal ophiolitic massif (eastern Cuba): Constraints on..., Lithos (2011), doi:10.1016/j.lithos.2011.01.016

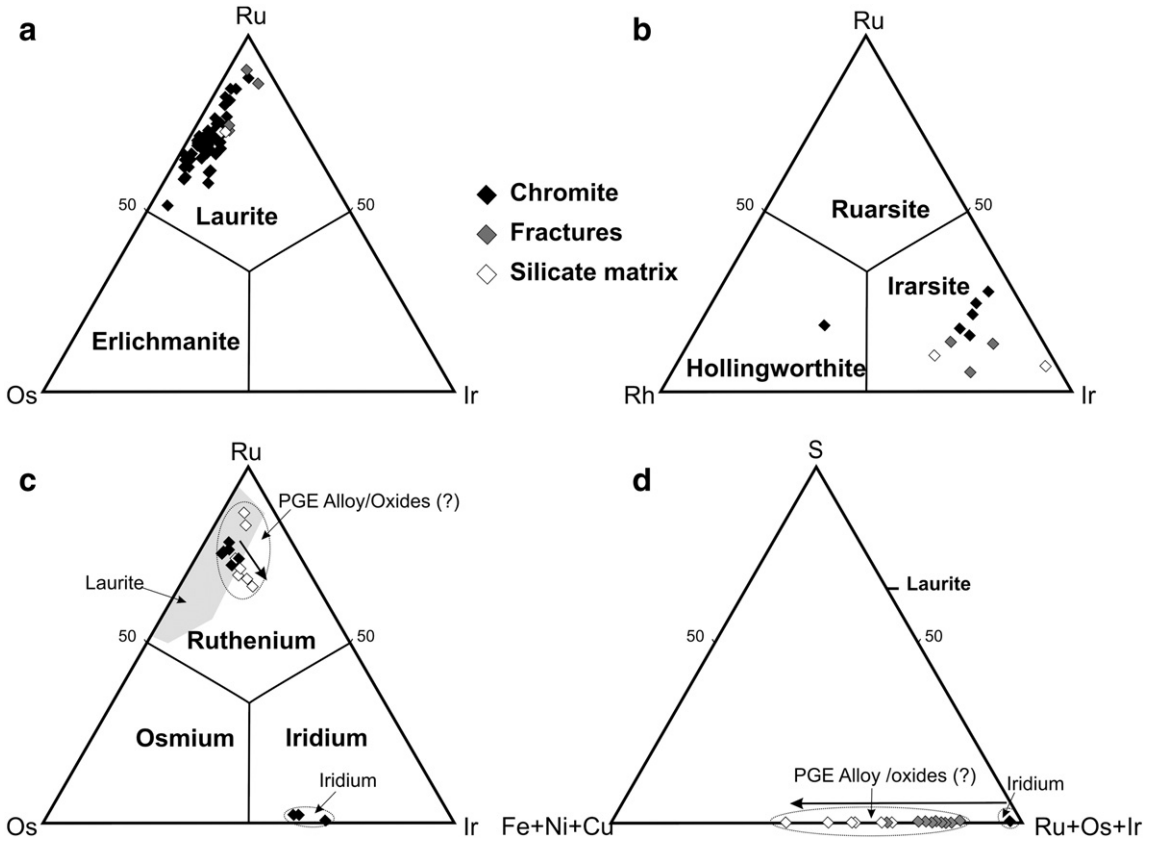

Fig. 10. Composition (at.%) of laurite (a), sulpharsenides of irarsite–hollingworthite solid solution series (b), and Ir–Ru–Os alloys and Ru–Os–Ir–Fe–Ni–(Rh) alloy/oxide (? (c and d)). Black arrows in (c) and (d) indicate chemical trends from chromite to fractures and silicate matrix, respectively.

the mixing/mingling of Cr-rich melts of boninitic affinity with variable degrees of differentiation within the dunitic melt flow channels (Lago et al., 1982) has caused saturation in chromian spinel producing monomineralic concentrations of chromite (Fig. 12a) (Irvine, 1977; Arai and Yurimoto, 1994; Zhou et al., 1996; Ballhaus, 1998). The fact that the primary chromian spinels show a wide range in composition within single chromitite bodies (Fig. 4) supports the idea that boninitic melts with variable compositions were involved during the genesis of the chromitites, which is predicted by a model for the formation of chromitites by the interplay of melt–rock and melt–melt interactions. High-Cr chromitites from Sagua de Tánamo have important Os-isotope heterogeneities at the metric, hand sample and section scales (Gervilla et al., 2005; Frei et al., 2006; Marchesi et al., 2010). This provides further evidence that boninitic melts with different composition, which very likely sampled Os from distinct mantle domains during melt–rock reactions, were involved in the formation of the chromitites. Oversaturation and/or concentration of high-Cr spinel during formation of the chromitites may have also been favored by the exsolution of fluid phases from these (olivine-saturated) melts (Fig. 12a) (Matveev and Ballhaus, 2002). Evidence of the role of water in the formation of the high-Cr chromitite is provided by the presence of amphiboles in the chromitite–dunite assemblage (i.e., interstitial chromitite matrix or as inclusions in chromian spinel of dunite) and in the harzburgite wall-rock (e.g., Melcher et al., 1997).

Table 6
Average (wt.%) Al_2O_3 and TiO_2 contents of chromite in chromitites of the Sagua de Tánamo district and calculated parental melts in equilibrium. Computations were made using the approaching of Kamenetsky et al. (2001) and Rollinson (2008) and the regression curves obtained by Zaccarini et al. (in press). Note that only data of chromitite samples not associated with gabbros were used for computation.

	Al_2O_3 spinel	TiO_2 spinel	Al_2O_3 melt	TiO_2 melt
High-Cr chromitites				
Tres Amigos	15.02	0.12	13.03	0.22
Guarina	14.75	0.22	12.91	0.33
Monte Bueno	15.88	0.28	13.33	0.39
Caridad	18.33	0.19	14.07	0.3
Tibera	18.58	0.16	14.15	0.27
Albertina	14.93	0.17	13.00	0.27
High-Al chromitites				
Negro Viejo	20.92	0.17	14.87	0.37
Demajagua	21.69	0.20	15.00	0.48
Cernícalo	24.04	0.18	15.44	0.43
Rupertina	27.19	0.16	15.94	0.33

In the Sagua de Tánamo high-Al chromitites, the relations between Cr# and TiO_2 show that the composition of the chromian spinel of chromitites covers a large area between the fields of IAT and MORB whereas the compositions of the chromian spinel of dunite and harzburgite cluster in a field specific to neither IAT nor MORB (Fig. 6b). This suggests a back-arc affinity, consistent with composition of the melt estimated to be in equilibrium with chromian spinel of the chromitite (i.e., back-arc basalt). Extrusive back-arc basin basalts having chromian spinel with a comparable chemistry to that in equilibrium with the parental melts of high-Al chromitites have not been reported yet in the Sagua de Tánamo area, but they have been found in some localities of the nearby Moa-Baracoa massif (i.e., Formation Morel and Quibijan) (Proenza et al., 2006; Marchesi et al., 2007). This may be interpreted in terms of the poor exposure or that such melts have never extruded as lavas. Our unpublished data show that these basalts were extracted from the mantle through "large" dunite bodies more than 100 m thick and 1 km long, which have chromian spinel with a similar composition to the chromian spinel of dunite hosting high-Al chromitites in the Sagua de Tánamo district.

Please cite this article as: González-Jiménez, J.M., et al., High-Cr and high-Al chromitites from the Sagua de Tánamo district, Mayarí-Cristal ophiolitic massif (eastern Cuba): Constraints on..., Lithos (2011), doi:10.1016/j.lithos.2011.01.016

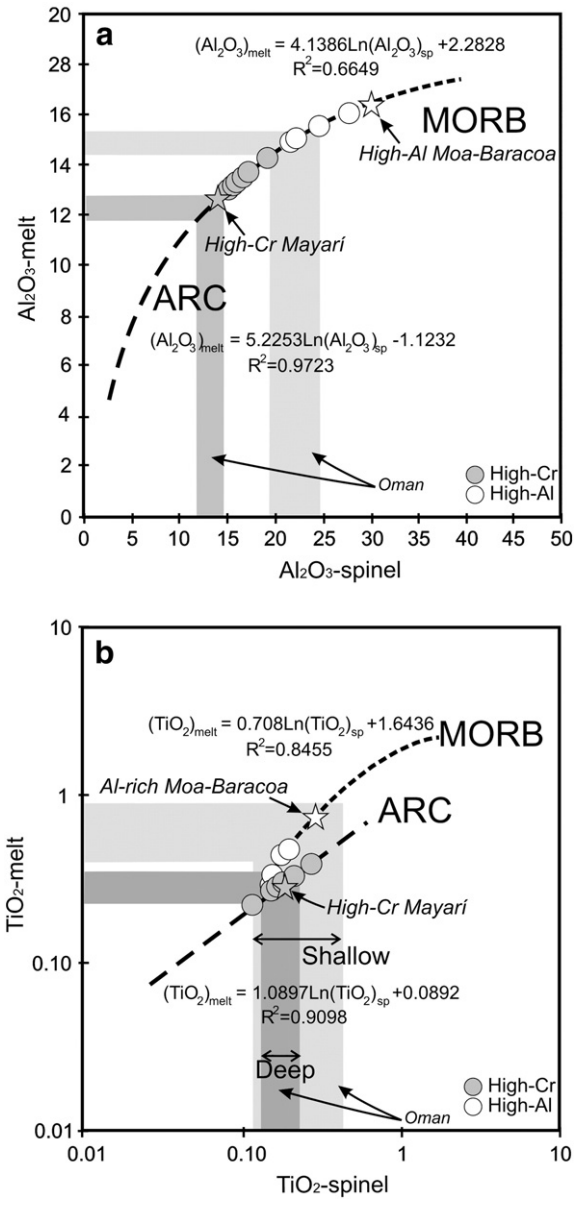

Fig. 11. Al_2O_3 (a) and TiO_2 (b) contents of the melt in equilibrium with Cr-rich and Al-rich chromitites from the Sagua de Tánamo, recovered from the regression lines obtained by Zaccarini et al. (in press) using data on chromite-melt inclusions in MORB and arc lavas reported by Kamenetsky et al. (2001) and Rollinson (2008). The range of chromite and the calculated melt compositions from the shallow and deep Wadi Rajmi chromitites in Oman (Rollinson, 2008) are shown for comparison. Only data of chromitite samples not associated with gabbros were used for computation.

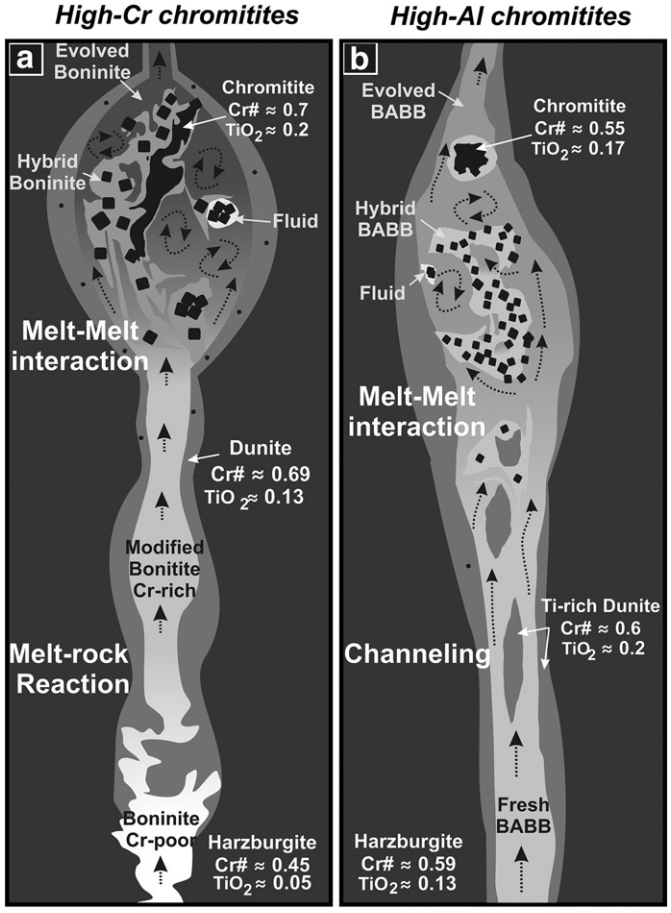

Fig. 12. Schematic cartoon illustrating the mechanism of formation of high-Cr (a) and high-Al (b) chromitites in the Sagua de Tánamo chromitites. Details are given in the main text.

The slight enrichment in Cr and Ti of spinel in dunite relative to spinel in harzburgite and chromitite (Figs. 6b and 12b) in the high-Al chromitites suggests that: (1) the formation of dunite involved the reaction of mantle harzburgite with BABB melt particularly enriched in Ti (e.g., Kelemen et al., 1999; Matsumoto and Arai, 2001) and that (2) chromitite and dunite were not formed in equilibrium from a common parental melt but the formation of chromitite required a back-arc basin basalt melt richer in Al and poorer in Ti than the one involved in dunite formation.

The subhedral to euhedral shape of chromian spinel in dunite and harzburgite hosting the high-Al chromitites suggests that the dunite is partly cumulative in origin (Matsumoto and Arai, 2001). Under relatively low melt/rock ratios, the reaction of ascending Ti-rich BABB melts with harzburgite may have generated residual dunite only along the boundary between melt and wall rock, thus producing chromian spinel with subhedral shapes in both harzburgite wall-rocks and dunite. Once the dunitic flow channel was formed, fractional crystallization may have dominated, as the melts moved less rapidly and cumulative dunite with predominantly euhedral chromian spinel was formed (e.g., Quick, 1981; Quick and Gergory, 1995; Kelemen et al., 1999; Matsumoto and Arai, 2001). As noted above, although large dunite bodies spatially associated with high-Al chromitites have not been found yet in Sagua de Tánamo, we have identified them in some parts of the nearby Moa-Baracoa massif.

At the P-T conditions (~1200 °C and ~0.5 Ga) under which chromitites formed in the mantle lithosphere (e.g., Ballhaus, 1998) the crystallization of high-Al chromian spinel occurs over a range of oxygen fugacity between −7 and −5 $\log_{10} fO_2$ (Hill and Roeder, 1974). At such conditions, back-arc basalts need an additional supply of silica and/or fluid component to enter the spinel + liquid field at around −7 $\log_{10} fO_2$. If these conditions are reached, the resulting melt is still relatively polymerized, making it difficult to percolate through the mantle harzburgite. In such a scenario, the melt tends to be focused through dunitic channels because they are more permeable than the harzburgite (e.g., Toramaru and Fuji, 1986; Kelemen et al., 1997, 1999). As the melt is not in equilibrium with olivine, during its percolation through dunite it will tend to dissolve olivine, producing melt-filled conduits in dunite. At increasing melt mass the combined effects of the reaction of the dissolution of olivine and injection of batches of more primitive BABB melts may have forced hybrid melts into the field of high-Al spinel in the spinel + liquid region of the olivine–silica–spinel system (e.g., Arai, 1997; Matsumoto et al., 1997). The interplay of olivine dissolution, and mixing/mingling of BABB melts with variable compositions may have produced high-Al chromian spinel with large ranges of composition

Please cite this article as: González-Jiménez, J.M., et al., High-Cr and high-Al chromitites from the Sagua de Tánamo district, Mayarí-Cristal ophiolitic massif (eastern Cuba): Constraints on..., Lithos (2011), doi:10.1016/j.lithos.2011.01.016

within single chromitite bodies (Fig. 4) as well as the important Os-isotope variations observed in these chromitites by Gervilla et al. (2005) and Frei et al. (2006). The supply of relatively oxidized fluids necessary to metasomatize harzburgite and to form relatively oxidized melts able to crystallize high-Al chromian spinel is again supported by the presence of amphibole in the chromitite–dunite–harzburgite (e.g., Melcher et al., 1997; Proenza et al., 1999).

8.3. Concentration and fractionation of PGE

In the Sagua de Tánamo chromitites, as in other ophiolitic chromitites, PGE abundance and Cr# show a roughly positive correlation (Fig. 8c) whereas bulk PGE content and the Pd/Ir ratio correlate negatively (Table 4). These relations indicate that PGE and the nature of the parental melt were closely related and that the presence of PGE-rich (i.e. high-Cr) and PGE-poor chromitites (i.e. high-Al) in the same mining district was a consequence of their crystallization from parental melts with different PGE contents. However, irrespective of their PGE abundances, both PGE-rich (high-Cr) and PGE-poor (high-Al) chromitites display a systematic enrichment in IPGE relative to PPGE (Fig. 8a and b). This distribution of the PGE in whole-rock is consistent with the PGM mineralogy observed in the chromitites, which is dominated by minerals of Ru, Os and Ir (mainly minerals of the laurite–erlichmanite solid solution series, and IPGE-oxides derived from them). This suggests that fractionation between IPGE and PPGE must have been related to the melting processes that affected mantle harzburgite before the generation of the chromitite, which was latterly reinforced by physical mechanisms of crystallization of PGM and host chromian spinel during the chromitite formation.

It is widely accepted that PGE are supplied to basaltic melts by the melting of residual sulfide, and to a lesser extent alloys, that reside in mantle peridotites (e.g., Lorand et al., 1999, 2010; Luguet et al., 2001; Alard et al., 2002; Büchl et al., 2002; Bockrath et al., 2004a). Thus, the PGE-signature of the melt is strongly dependent on the melt regime and the stages of melting of these carrier phases. In ophiolite settings, arc-related melts that form above the subduction slab are generated by moderate to high degrees of partial melting (i.e., ≥20%), which produce nearly complete dissolution of mantle sulfides, giving rise to basaltic melts enriched in PGE. As a consequence the chromitites formed in equilibrium with such melts tend to be PGE-rich with contents from a hundred to thousands of ppb (e.g., Konstantopoulou and Economou-Eliopoulos, 1991; Economou-Eliopoulos, 1996; Zhou et al., 1998; Proenza et al., 1999; Ahmed and Arai, 2002; Gervilla et al., 2005; Prichard et al., 2008; Uysal et al., 2009a).

However, basaltic melts that form beneath spreading centers (i.e., mid-ocean ridges or back-arc basins) are generated at lower degrees of partial melting, usually less than 20%, which is not sufficient to remove all mantle sulfide, and thus produce melts with very low levels of PGE. The chromitites crystallized in equilibrium with these melts usually have extremely low PGE concentrations around a few ppb (e.g., Graham et al., 1996; Economou-Eliopoulos, 1996; Zhou et al., 1998; Proenza et al., 1999, 2004, 2008; Ahmed and Arai, 2002; Gervilla et al., 2005; Uysal et al., 2007, 2009a). A recent study of PGE concentrations in a set of chromitites of the Al'Ays ophiolite complex (Prichard et al., 2008) and literature data indicate that chromitites enriched in PGE crystallized in equilibrium with melts formed in a critical melting interval at around 20–25%. This also suggests that melts generated by lower melting degrees will tend to form PGE-poor chromitites; if degrees of melting are beyond the critical interval, the melts will be diluted in the volatile PGE (i.e., Pt and Pd) thus producing PGE-rich chromitites practically barren of Pt and Pd.

In the Sagua de Tánamo district, high-Cr chromitites have relatively high PGE contents (mean ~2000 ppb) and appreciable amounts of Pt and Pd (up to 250 ppb). This suggests that the melting of the mantle peridotite was high enough to enter the critical melting interval for the effective extraction of PGE from removal of mantle sulfides, but did not extend beyond this interval to dilute the parental melts in the refractory PPGE. In contrast, the PGE-poor nature of the high-Al chromitites suggests degrees of melting lower than for the high-Cr chromitites, but high enough to enter the critical interval and concentrate some PGE (mean ~100 ppb).

As the parental melts of the chromitites percolated through an already depleted peridotite (Marchesi et al., 2006), which was affected by previous events of partial melting (Frei et al., 2006; Marchesi et al., 2010), it would be expected that sulfides (ideally containing all six PGE) hosted in the pristine mantle peridotite also underwent partial melting. As a result, the sulfide left behind in the residual depleted harzburgite during the successive partial melting events, as experimentally shown Bockrath et al. (2004a), must have been enriched in Os, Ir and Ru, but moderately depleted in Rh, Pt and Pd. If these residual sulfides were removed during melt–rock reaction related to the formation of chromitites, their fractionated PGE nature must have been transferred to the migrating parental basaltic melts (Büchl et al., 2002; Bockrath et al., 2004a). This mechanism can explain the similar PGE patterns of the two chromitite varieties (Fig. 8a and b). The positive correlation between PGE and Cr# (and thickness of the dunite selvages) (Fig. 8C) suggests that, as for Cr, PGE were more effectively concentrated in high-Cr chromitites, and it may be related to the extent of melt–rock reactions associated with the formation of the chromitite–dunite. Thus, we suggest that with increasing melt volume, the parental boninitic melts of high-Cr chromitites (already enriched in PGE from their source) must have dissolved during their migration a significant volume of mantle sulfides, becoming richer in PGE (and Cr) and explaining the positive correlation between PGE and Cr#.

In contrast, the relatively fast channeling of the parental BABB melts of high-Al chromitites (relatively PGE-poor) through conduits in dunite prevented any appreciable interaction with harzburgite wall-rocks, thus preventing the melts from assimilating more PGE than were in their source. Thus the concentration of PGE in the parental melts of chromitites could be related not only to the degree of partial melting at the source of the parental melt, but also to the extent of reaction between the migrating melt and the host harzburgite during the formation of the chromitite. Once the PGE were released into the silicate melt, their fractionation was governed only by their solubility in the melt.

Experimental data suggest at S-undersaturated conditions in chromian spinel-saturated systems, like the parental melts of ophiolitic chromitites, the fractionation of PGE may be controlled by crystallization of chromian spinel. Because the spinel selectively takes up trivalent Cr, Al, and Fe from the melt relative to divalent species, each nucleus of growing spinel may develop a reduced zone at the melt–crystal interface (Mungall, 2002, 2005). The perturbation of fO_2 in the compositional boundary layer may lower the solubility of the most oxidized species – i.e., Ru, Os and Ir – causing their saturation, then precipitating submicroscopic grains (or clusters) of these elements in metallic state (Finnigan et al., 2008). In such a scenario, the presence of chromian spinel provides a nucleation substrate for these refractory PGE alloys (Ballhaus et al., 2006). Changes in fO_2 and/or fS_2 in the melt as a consequence of melt–rock reaction or melt–melt interaction may promote the formation of IPGE-bearing sulfides by reaction with the already formed IPGE alloys (Bockrath et al., 2004b; González-Jiménez et al., 2009b). During coarsening by a coalescence of chromian spinel nuclei, the alloy micro-nuggets and the larger sulfides become mechanically trapped within chromian spinel grains (e.g., Augé, 1985; Melcher et al., 1997; Gervilla et al., 2005). In this model, the small amount of Pt and Pd available in the parental silicate melt tend to remain dissolved metastably because of their lower affinity for the spinel; Pt- and Pd-rich minerals thus tend predominantly to crystallize on the edges of spinel grains or in the silicate matrix. Rh may have a behavior somewhere between the end members Os–Ir–Ru and

Please cite this article as: González-Jiménez, J.M., et al., High-Cr and high-Al chromitites from the Sagua de Tánamo district, Mayarí-Cristal ophiolitic massif (eastern Cuba): Constraints on..., Lithos (2011), doi:10.1016/j.lithos.2011.01.016

Pt–Pd (Ballhaus et al., 2006). This mechanism for the separation of the PGE has been demonstrated experimentally (e.g., Finnigan et al., 2008; Ballhaus et al., 2006) and matches well with the observed distribution of PGM in the Sagua de Tánamo chromitites and in other mantle-related ophiolitic chromitites worldwide; Os–Ir–Ru minerals are preferentially included in chromian spinel, Rh-bearing minerals occur both inside chromian spinel or in the silicate matrix and Pt- and Pd-rich minerals are absent or occur in the silicate matrix of the chromitites (e.g., Prichard et al., 2008; González-Jiménez et al., 2009a).

8.4. Origin of the PGM assemblages

The absence of primary Os-rich alloys in the Sagua de Tánamo chromitites suggests that in the earlier magmatic stages when chromian spinel was precipitating, sulfur fugacity was high enough to accommodate most available Os in the structure of laurite and/or erlichmanite (Brenan and Andrews, 2001; Andrews and Brenan, 2002; Bockrath et al., 2004b). Laurite–erlichmanite grains included in chromian spinel of the Sagua de Tánamo chromitites commonly have euhedral shapes indicative of direct (i.e., free) crystallization from a basaltic melt (e.g., Augé, 1985; Ahmed and Arai, 2003). However, the fact that some primary grains of iridium, occur rimed by kashinite (?) (Fig. 9d), indicates that in some cases IPGE-bearing sulfides could have formed as result of the sulfurization of a precursor alloy, as fS_2 increased in the melt. This observation provides strong evidence for the mechanism of fractionation of PGE as result of the early segregation of IPGE alloys. Textures supporting a secondary origin of the laurite–erlichmanite by breakdown of Ru–Os-bearing alloys have not been seen in the Sagua de Tánamo chromitites, although it would be expected as experimentally shown Bockrath et al. (2004b) and described Grieco et al. (2006) in chromitites from the Nurali Massif in southern Urals. Breakdown of IPGE alloys due to rising fS_2 could occur as a response to decreasing temperature upon cooling of the parental melt of the chromitites (Augé and Johan, 1988; Garuti et al., 1999; Grieco et al., 2006). However, the complex zoning exhibited by some grains of laurite–erlichmanite (with drop-like inclusions of BMS) and irarsite–hollingworthite (Fig. 9c) indicates short-lived changes of the chemistry (i.e. fS_2 and aAs) and temperature in the melt during the formation of the PGM (González-Jiménez et al., 2009b). Such fluctuations could be produced by the interplay of melt–rock reaction and/or melt mixing/mingling. In such a scenario, PGM and BMS, stable within a wide range of fS_2 and temperature, could have crystallized simultaneously in different zones of the dunitic channel in which chromitites were formed. This may explain the coexistence of PGM typical of S-undersaturated conditions (i.e. laurite–erlichmanite and iridium) with other PGM (i.e. cuproiridsite) or Ni–Fe–Cu sulfides derived from crystallization of droplets of immiscible sulfide melts.

Grains of laurite located in ferrian chromite rims or along fractures filled by secondary silicates have irregular shapes as well as lower contents of S and Os compared to laurite included in the unaltered cores of chromian spinel. A similar contrast of shape and variation of the chemistry between primary unaltered and secondary "altered" laurite has been described in other ophiolitic chromitites: Shetland in Scotland (Prichard et al., 1986; Tarkian and Prichard, 1987), Tehuitzingo in Mexico (Zaccarini et al., 2005) and Dobromirtsi in Bulgaria (González-Jiménez et al., 2010). Such variations were interpreted by these authors as result of the desulfurization/oxidation of laurite by hydrothermal alteration related to serpentinization. Data on H/D and, O and C isotopes (Proenza et al., 2003) provided evidence that the Mayarí-Cristal peridotites were intensively serpentinized in a sub-ocean floor environment. During serpentinization laurite grains sited along the edges of chromian spinels interacted with alteration fluids. As a result they were partially dissolved and lost some S and Os. In some cases the fracturing or dissolution of the host chromian spinel released the laurite inclusions to the silicate matrix. A further interaction of already-altered laurite with circulating fluids leached most of the S, producing secondary Ru–Os–Ir–Fe–Ni–(Rh) alloy/oxides (?). This interpretation is supported by the similar Ru/Os ratio of laurite and the Ru–Os–Ir–Fe–Ni–(Rh) alloy/oxides (?) and the linear outlines of the latter minerals suggest that they pseudomorph pre-existing laurite (e.g., Stockman and Hlava, 1984; Garuti and Zaccarini, 1997; Prichard et al., 2008). The higher content of base-metals in Ru–Os–Ir–Fe–Ni–(Rh) alloy/oxides (?) located in the silicate matrix in comparison with those located in fractures suggests a small-scale remobilization of PGE by fluids related to serpentinization, balanced by the addition of base metals as observed in other secondary assemblages of IPGE-rich PGM in ophiolitic chromitites (e.g., Garuti and Zaccarini, 1997; Proenza et al., 2007).

The occurrence of anhedral irarsite–hollingworthite in the altered zones of the Sagua de Tánamo chromitites may be interpreted as a result of alteration *in situ* of pre-existing magmatic grains or as a neo-formation by fixing of remobilized components during serpentinization (Thalhammer et al., 1990; Malitch et al., 2001; González-Jiménez et al., 2010). In this study the few grains of these species found do not permit a conclusive interpretation. Nevertheless, applying the proposed model for fractionation between PGE in chromitites during the magmatic stage, it is reasonable that irarsite–hollingworthite originally was magmatic grains located on the edges of chromian spinel or in the interstitial silicate matrix. Thus they were very likely altered *in situ* during serpentinization (e.g., Prichard et al., 2008). Alteration implies dissolution along grain boundaries, some loss of S and in some cases remobilization of Ru and Os with a slight residual enrichment in Pt, supportive of partial re-crystallization of some grains during serpentinization (González-Jiménez et al., 2010). Further evidence for the crystallization of As-bearing phases during serpentinization is the occurrence of orcelite exclusively in the serpentinized silicate matrix.

8.5. Coexistence of high-Cr and high-Al chromitites in the small district of Sagua de Tánamo

The coexistence of high-Cr and high-Al chromitites is a common feature of many ophiolitic belts. The two chromitite varieties may occur in separated massifs (e.g., Leblanc and Violette, 1983; Zhou and Bai, 1992; Graham et al., 1996; Economou-Eliopoulos, 1996; Zhou et al., 1994, 1996, 1998; Proenza et al., 1999; Ahmed et al., 2001; Tsoupas and Economou-Eliopoulos, 2008; Uysal et al., 2009a) or less frequently interspersed within a single ultramafic massif containing variably depleted peridotites (e.g., Thayer, 1964; Ahmed, 1984; Leblanc, 1995; Proenza et al., 1999; Melcher et al., 1997; Zaccarini et al., in press). A bimodal distribution and vertical zoning have been observed in some cases, with high-Al chromitites being located towards the petrological Moho and high-Cr chromitites in deeper parts of the mantle section (e.g., Leblanc and Violette, 1983; Roberts and Neary, 1993; Ahmed and Arai, 2002; Rollinson, 2008). The coexistence of both types of chromitites has been interpreted as due to: (1) melts that originated in different magmatic sources of the ophiolite environment (i.e., MOR, SSZ and Arc regions) at different times during the formation and/or evolution of oceanic lithosphere (e.g., Melcher et al., 1997; Zhou and Robinson, 1997; Zhou et al., 1998; Ahmed and Arai, 2002; Uysal et al., 2009a), (2) contrasting behavior of ultramafic rocks and upwelling mafic melts (i.e., melt–rock reactions by infiltration vs. channeling) along major tectonic discontinuities (e.g., paleotransform faults; Leblanc, 1995), (3) progressively fractionating parental melts, initially Cr-rich in SSZ and Arc regions (e.g., Graham et al., 1996; Zaccarini et al., in press).

At Sagua de Tánamo, chromitites occur interspersed in a narrow zone less than 3 km long (Fig. 1). However, there is little scope to estimate the original stratigraphic distances among chromitite bodies because of the poor exposure in the tropical forest and pervasive faulting. Despite the lack of outcrop, available regional mapping suggests that the chromitite-bearing peridotites occur as imbricated

Please cite this article as: González-Jiménez, J.M., et al., High-Cr and high-Al chromitites from the Sagua de Tánamo district, Mayarí-Cristal ophiolitic massif (eastern Cuba): Constraints on..., Lithos (2011), doi:10.1016/j.lithos.2011.01.016

tectonic sheets. Faulting and thrusting both can explain the coexistence of different types of chromitites hosted in peridotite with different degrees of depletion within a small area. However, despite the possible effects of tectonics, the nearly continuous spectrum of composition of the chromitites (e.g., Fig. 11a) is more consistent with a progressively changing (with time and space) melt source. Thus, the occurrence of both types of chromitites in variably depleted peridotite (i.e., high-Cr chromitites in less refractory and high-Al in more refractory) in Sagua de Tánamo suggests that the ascending parental melts of chromitites traveled through and were emplaced within a geochemically segmented lithosphere, as suggested by Rollinson (2008) in the case of the Oman chromitites (see Fig. 5). This interpretation is consistent with the Os-isotope data on the Sagua de Tánamo chromitites, which indicate that parental melts of the Sagua de Tánamo chromitites sampled mantle domains that had experienced a protracted history of partial melting events (Gervilla et al., 2005; Frei et al., 2006; Marchesi et al., 2010).

The close association of harzburgites showing variable degrees of depletion/metasomatism is a feature of back-arc basins developed in supra-subduction zone environment (e.g., Keller et al., 2008; Metcalf and Shervais, 2008; Rollinson, 2008 and references therein) where regions of greater and lesser melt extraction/percolation may coexist on a scale of a few kilometers. Arc-melts of IAT and/or BABB affinity can be coevally derived from, and/or become emplaced in, variably metasomatized mantle peridotites (e.g., Vailler et al., 1991; Kamenetsky et al., 1997; Cluzel et al., 2010). Thus, we suggest that the present distribution of high-Cr and high-Al chromitites in the small mining district of Sagua de Tánamo reflects temporal and/or spatial variations in the types of melt that were generated from, and emplaced in, a range of subarc mantle domains during opening of a back-arc basin in a supra-subduction zone environment. In Sagua de Tánamo the existence of a transitional (IAT to MORB) back-arc mantle in Cretaceous times has recently been firmly established on geochemical (Marchesi et al., 2006, 2007, 2010; Proenza et al., 2006) and paleontological evidence (Iturralde-Vinent et al., 2006).

9. Conclusions

(1) Podiform chromitites containing chromian spinel with a large spectrum of compositions, from high-Cr to high-Al, occur interspersed within a small area (<3 km long) in the Sagua de Tánamo district, Mayarí-Cristal Ophiolitic massif, eastern Cuba.

(2) The bimodal compositional distribution of the chromian spinel in the chromitite coincides with variations in the composition of chromian spinel and silicates of the enclosing dunite cocoons and harzburgite wall-rocks. In high-Cr chromitites the chromitite and dunite crystallized from a common parental boninite-like melt, as a result of reaction between mantle harzburgite with a percolating island arc tholeiite melt coupled with related melt mixing/mingling within the dunite created by melt–rock reaction. Large variations in the chemistry of chromian spinel, types of PGM and BMS assemblages, and heterogeneities in the Os-isotopes of the chromitite, support this interpretation. On the other hand, in high-Al chromitites, chemistry of chromian spinel suggests that chromitite and dunite did not crystallize in equilibrium, and the chromitites formed from more Al-rich melts than the dunite. Similar variations in the chemistry of chromian spinel and Os-isotope distribution also suggests a mechanism of mixing/mingling of BABB melt with variable composition. In this case, melt–melt interaction occurred within conduits in dunite created by the dissolution of olivine when primitive BABB melt percolated through pre-existing dunitic channels.

(3) The chromitites show a rough positive correlation between the chemistry of chromian spinel and the abundance of PGE and PGM in the chromitite. High-Cr chromitites are richer in PGE and PGM than high-Al ones. Nevertheless, irrespective of their total PGE contents all the chromitites show a systematic enrichment in IPGE relative to PPGE, as is typical of ophiolitic podiform chromitites. This distribution of PGE is controlled by the suite of PGM, which is dominated by minerals of Ru, Os and Ir, mainly minerals of the laurite–erlichmanite solid solution series. This suggests a close link between the extraction IPGE and PPGE from the mantle, and their subsequent crystallization. Fractionation between IPGE and PPGE was related to melting processes that affected mantle harzburgite before chromitite genesis, which was later reinforced by the crystallization of PGM and host chromian spinel during the chromitite formation. Concentration of PGE in to the melt was related to the variable extent of removal of sulfides during chromitite formation.

(4) The coexistence of high-Cr and high-Al chromitites is interpreted as reflecting temporal and/or spatial variations of separate melt intrusions, originating from different mantle sources, and emplaced in a geochemically segmented lithosphere across subarc mantle domains, during the opening of a back-arc basin in a suprasubduction zone environment.

Acknowledgements

We wish to acknowledge the assistance of A. Rueda Torres (Department of Mineralogy and Petrology, University of Granada) in the preparation of the polished sections and the assistance of X. Llovet (Serveis Científicotècnics of the University of Barcelona), I. Sánchez Almazo (Centro Andaluz de Medio Ambiente of the Junta Andalucía-University of Granada), A. González Segura (Centro de Instrumentación Científica of the University of Granada) for their assistance with EPMA, ESEM and FESEM, respectively. The authors are also grateful to I. F. Blanco-Quintero (University of Granada) for his help in understanding subduction processes in the Caribbean area which greatly improved this manuscript. S. Arai (University of Kanazawa, Japan) and an anonymous reviewer are acknowledged for their criticism that greatly improved our manuscript. Editor in-Chief and Journal Manager of Lithos Ruud Koole and Nelson Eby are also thanked by helping the final editing of the manuscript. This research has been supported by the Spanish projects CGL2007-61205and CGL2009-10924, and the research group (RNM 131) of the Junta de Andalucía, grant 2009-SGR444 of the Catalonian Government, and F.P.I grant BES-2005-8328 of the Spanish Ministry of Education and Sciences. Part of the analytical data were obtained using instrumentation funded by ARC LIEF, and DEST, Systemic Infrastructure Grants, industry partners and Macquarie University. This is contribution 705 from the Australian Research Council National Key Centre for the Geochemical Evolution and Metallogeny of Continents (http://www.gemoc.mq.edu.au).

References

Ahmed, A.H., Arai, S., 2002. Unexpectedly high-PGE chromitite from the deeper mantle section of the northern Oman ophiolite and its tectonics implications. Contributions to Mineralogy and Petrology 143, 263–278.

Ahmed, A.H., Arai, S., 2003. Platinum-group minerals in podiform chromitites of the Oman ophiolite. Canadian Mineralogist 41, 597–616.

Ahmed, A.H., Arai, S., Attia, A.K., 2001. Petrological characteristics of podiform chromitites and associated peridotites of the Pan African Proterozoic ophiolite complexes of Egypt. Mineralium Deposita 36, 72–84.

Ahmed, Z., 1984. Stratigraphic and textural-variation in the chromite composition of the ophiolitic Sakhakot-Qila complex, Pakistan. Economic Geology 79, 1334–1359.

Alard, O., Griffin, W.L., Pearson, N.J., Lorand, J.-P., O'Reilly, S.Y., 2002. New insights into the Re–Os systematics of sub-continental lithospheric mantle from in situ analysis of sulphides. Earth and Planetary Science Letters 203, 651–663.

Andrews, D.R.A., Brenan, J.M., 2002. Phase-equilibrium constraints on the magmatic origin of laurite + Ru–Os–Ir alloy. Canadian Mineralogist 40, 1705–1716.

Arai, S., 1992. Petrology of peridotites as a tool of insight into mantle processes: a review. Journal of Petrology of Economic Geology 87, 351–363 (in Japanese with English abstract).

Please cite this article as: González-Jiménez, J.M., et al., High-Cr and high-Al chromitites from the Sagua de Tánamo district, Mayarí-Cristal ophiolitic massif (eastern Cuba): Constraints on..., Lithos (2011), doi:10.1016/j.lithos.2011.01.016

Arai, S., 1997. Control of wall-rock composition on the formation of podiform chromitites as a result of magma/peridotite interaction. Resource Geology 47, 177–187.

Arai, S., Yurimoto, H., 1994. Podiform chromitites of the Tari-Misaka ultramafic complex, Southwest Japan, as mantle–melt interaction products. Economic Geology 89, 1279–1288.

Arai, S., Yurimoto, H., 1995. Posible subarc origin of podiform chromitites. The Island Arc 4, 104–111.

Augé, T., 1985. Platinum-group mineral inclusions in ophiolitic chromitite from the Vourinos Complex, Greece. Canadian Mineralogist 23, 163–171.

Augé, T., 1988. Platinum-group minerals in the Tiébaghi and Vourinos ophiolite complexes: genetic implications. Canadian Mineralogist 26, 177–192.

Augé, T., Johan, Z., 1988. Comparative Study of Chromite Deposits from Troodos, Vourinos, North Oman and New Caledonia Ophiolites. In: Boissonnas, J., Omenetto, P. (Eds.), Mineral Deposits in the European Community. Springer-Verlag, Heidelberg, pp. 267–288.

Ballhaus, C., 1998. Origin of podiform chromite deposits by magma mingling. Earth and Planetary Science Letters 156, 185–193.

Ballhaus, C., Bockrath, C., Wohlwgemuth-Uberwasser, C., Laurenz, V., Berndt, J., 2006. Fractionation of the noble metals by physical processes. Contributions to Mineralogy and Petrology 152, 667–684.

Bédard, J.H., Hébert, R., 1998. Formation of chromitites by assimilation of crustal pyroxenites and gabbros into peridotitic intrusions: North Arm Mountain massif, Bay of Islands ophiolite, Newfoundland, Canada. Journal of Geophysical Rearch 103, 5165–5184.

Blanco-Quintero, I.F., Proenza, J.A., García-Casco, A., Tauler, E., Galí, S., 2011. Serpentinites and serpentinites within a fossil subduction channel: La Corea mélange, eastern Cuba. Geologica Acta 9, 2–3.

Bockrath, C., Ballhaus, C., Holzheid, A., 2004a. Fractionation of the platinum-group elements during mantle melting. Science 305, 1951–1953.

Bockrath, C., Ballhaus, C., Holzheid, A., 2004b. Stabilities of laurite RuS_2 and monosulphide liquid solution at magmatic temperature. Chemical Geology 208, 265–271.

Brenan, J.M., Andrews, D., 2001. High-temperature stability of laurite and Ru–Os–Ir alloy and their role in PGE fractionation in mafic magmas. Canadian Mineralogist 39, 341–360.

Büchl, A., Brügmann, G., Batanova, V.G., Münker, C., Hofmann, A.W., 2002. Melt percolation monitored by Os isotopes and HSE abundances: a case study from the mantle section of the Troodos Ophiolite. Earth and Planetary Science Letters 204 (3–4), 385–402.

Cabri, L.J., 2002. The Geology, Geochemistry, Mineralogy and Mineral Beneficiation of Platinum-Group Minerals. Canadian Institution of Mining Metal and Petroleum, Calgary, Alberta, Canada. pp. 852.

Carmichael, I.S.E., 1967. The iron-titanium oxides of salic volcanic rocks and their associated ferromagnesian silicates. Contributions to Mineralogy and Petrology 14, 36–64.

Cluzel, D., Black, P.M., Picard, C., Nicholson, K.N., 2010. Geochemistry and tectonic setting of Matakoa volcanic (East Coast Allocton, New Zealand); suprasubduction zone affinity, regional correlations and origin. Tectonics 29 (TC2013) doi:10.1029/20089TC002454 21 p.

Crawford, A.J., Fallon, T.J., Green, D.H., 1989. Classification, Petrogenesis and Tectonic Setting of Boninites. In: Crawford, A.J. (Ed.), Unwin and Hyman, London, pp. 2–44.

Dick, H.J.B., Bullen, T., 1984. Chromian spinel as a petrogenetic indicator in abyssal and alpine-type peridotites and spatially associated lavas. Contributions to Mineralogy and Petrology 86, 54–76.

Economou, M., 1983. Platinum group melts in chromite ores from the Vourinos Ophiolite Complex, Greece. Ofioliti 8, 339–356.

Economou-Eliopoulos, M., 1996. Platinum-group element distribution in chromite ores from ophiolite complexes: implications for their exploration. Ore Geology Reviews 11, 363–381.

Economou, M., Dimou, E., Economou, G., Migiros, G., Vacondios, I., Grivas, E., Rassios, A., Dabitzias, S., 1986. Chromite Deposits of Greece. In: Johan, Economou, M. (Eds.), Metallogeny of Ophiolites. UNESCO IGCP 197 Project. Theoprastus, Athens, pp. 129–160.

Edwards, S.J., Pearce, J.A., Freeman, J., 2000. New Insights Concerning the Influence of Water During the Formation of Podiform Chromite. Boulder In: Dilek, Y., Moores, E.M., Elthon, D., Nicolas, A. (Eds.), Ophiolites and Oceanic Crust: New Insights from Field Studies and the Ocean Drilling Program: Geological Society of America. Special Paper, vol. 349, pp. 139–147.

Finnigan, C.S., Brenan, J.M., Mungall, J.E., McDonough, W.F., 2008. Experiments and models bearing on the role of chromite as a collector of platinum group minerals by local reduction. Journal of Petrology 49, 1647–1665.

Fonseca, E., Zelepugin, V.N., Heredia, M., 1985. Structure of the ophiolite association of Cuba. Geotectonic 19, 321–329.

Frei, R., Gervilla, F., Meibom, A., Proenza, J.A., Garrido, C.J., 2006. Os isotope heterogeneity of the upper mantle: evidence from the Mayarí–Baracoa ophiolite belt in eastern Cuba. Earth and Planetary Science Letters 241, 466–476.

García-Casco, A., Iturralde-Vinent, M.A., Pindell, J., 2008. Latest Cretaceous collision/accretion between the Caribbean Plate and Caribeana: origin of metamorphic terranes in the Greater Antilles. International Geology Review 50, 781–809.

García-Casco, A., Torres-Roldán, R.L., Iturralde-Vinent, M.A., Millán, G., Núñez-Cambra, K., Lázaro, C., Rodriguez-Vega, A., 2006. High pressure metamorphism of ophiolites in Cuba. Geological Acta 4, 63–88.

Garuti, G., Zaccarini, F., 1997. In situ alteration of platinum-group minerals at low temperature: evidence from serpentinized and weathered chromitite of the Vourinos complex, Greece. Canadian Mineralogist 35, 611–626.

Garuti, G., Zaccarini, F., Cabella, R., Fershtater, G., 1997. Ocurrence of unkown Ru–Os–Ir–Fe oxides in the chromitites of the Nurali ultramafic complex, southern Urals, Russia. Canadian Mineralogist 35, 1431–1439.

Garuti, G., Zaccarini, F., Moloshag, V., Alimov, V., 1999. Platinum-group elements as indicators of sulphur fugacity in ophiolitic upper mantle: an example from chromitites of the Ray-Iz ultramafic complex, Polar Urals, Russia. Canadian Mineralogist 37, 1099–1115.

Gervilla, F., Proenza, J.A., Frei, R., González-Jiménez, J.M., Garrido, C.J., Melgarejo, J.C., Meibom, A., Díaz-martínez, R., Lavaut, W., 2005. Distribution of platinum-group elements and Os isotopes in chromite ores from Mayarí-Baracoa Ophiolilte Belt (eastern Cuba). Contributions to Mineralogy and Petrology 150, 589–607.

Ghosh, B., Pal, T., Bhattacharya, A., Das, D., 2009. Petrogenetic implications of ophiolitic chromite from Rutland Island, Andaman—a boninitic parentage in supra-subduction setting. Mineralogy and Petrology 96, 59–70.

González-Jiménez, J.M., Gervilla, F., Kerestedjian, T., Proenza, J.A., 2010. Effects of metamorphism on platinum-group and base-metal mineral assemblages in ophiolite chromitites from the Dobromirtsi massif, Rhodope Mountais (SE Bulgaria). Resources Geology 60 (4), 315–334.

González-Jiménez, J.M., Gervilla, F., Proenza, J.A., Augé, T., Kerestedjian, T., 2009a. Distribution of platinum-group minerals in ophiolitic chromitites. Applied Earth Section B (Transactions Institution Mining and Metallurgy) 118, 101–110.

González-Jiménez, J.M., Gervilla, F., Proenza, J.A., Kerestedjian, T., Augé, T., Bailly, L., 2009b. Zoning of laurite (RuS_2)-erlichmanite(OsS_2): implications for the genesis of PGM in ophiolite chromitites. European Journal of Mineralogy 21 (2), 419–432.

Graham, I.T., Franklin, B.J., Marshall, B., 1996. Chemistry and mineralogy of podiform chromitite deposits, southern NSW, Australia: a guide to their origin and evolution. Mineralogy and Petrology 37, 129–150.

Grieco, G., Diella, V., Chaplygina, N.L., Savalieva, G.N., 2006. Platinum group elements zoning and mineralogy of chromitite from the cumulate sequence of the Nurali massif (Southern Urals, Russia). Ore Geology Review 30 (1–3), 257–276.

Hattori, K.H., Takahashi, Y., Augé, T., 2010. Mineralogy and origin of oxygen-bearing platinum–iron grains based on an X-ray absorption spectroscopy study. American Mineralogist 95, 622–630.

Hicky, R.L., Frey, F.A., 1982. Geochemical characteristics of boninite serives volcanic: implication for their source. Geochimica et Cosmochimica Acta 46, 2099–2115.

Hill, R., Roeder, P., 1974. The crystallization of spinel from basaltic liquids as a function of oxygen fugacity. Journal of Geology 82, 709–729.

Irvine, T.N., 1977. Origin of chromitite in the Muskov intrusion and other stratiform intrusions: a new interpretation. Geology 5, 273–277.

Iturralde-Vinent, M.A., Díaz-Otero, C., Roríguez-Vega, A., Díaz-Martínez, R., 2006. Tectonic implications of paleontologic dating of Cretaceous–Danian sections of Eastern Cuba. Geological Acta 4, 89–102.

Kamenetsky, V.S., Crawford, A., Eggins, S., Mühe, R., 1997. Phenocryst and melt inclusion chemistry of near-axis seamounts, Valu Fa Ridge, Lau Basin: insight into mantle wedge melting and the addition of subduction components. Earth and Planetary Sciences 151, 205–223.

Kamenetsky, V.S., Crawford, A.J., Meffre, S., 2001. Factors controlling chemistry of magmatic spinel: an empirical study of associated olivine, Cr-spinel and melt inclusions from primitive rocks. Journal of Petrology 42, 655–671.

Kelemen, P.B., 1990. Reaction between ultramafic rock and fractionating basaltic magma. I. Phase relations, the origin of calc-alkaline magma series, and the formation of discordant dunite. Journal of Petrology 31, 51–98.

Kelemen, P.B., Koga, K., Shimizu, N., 1997. Geochemistry of gabbro sills in the crust-mantle transition zone of the Oman ophiolite: implications for the origin of the oceanic lower crust. Earth and Planetary Sciences Letters 146, 475–488.

Kelemen, P.B., Hirth, G., Shimizu, N., Spiegelman, M., Dick, H.J.B., 1999. A Review of Melt Migration Processes in the Adiabatically Upwelling Mantle Beneath Oceanic Spreading Ridges. In: Cann, J.D., Elderfield, H., Laughton, A.A. (Eds.), Mid-Ocean Ridges, Dynamics or Processes Associated with Creation of new Ocean Crust. Cambridge, pp. 67–102.

Keller, N.S., Arculus, R.J., Hermann, J., Richards, S., 2008. Submarine back-arc lava with arc signature: Fonualei Spreading Center, northeast Lau Basin, Tonga. Journal of Geophysical Research 113, B08S07 doi:10.1029/2007JB005451.

Kocks, H., Melcher, F., Meisel, T. And, Burgath, K.P., 2007. Diverse contributing sources to chromitite petrogenesis in the Shebenik Ophiolitic Complex, Albania: evidence from new PGE- and Os-isotope data. Mineralogy and Petrology 91, 139–170.

Konstantopoulou, G., Economou-Eliopoulos, M., 1991. Distribution of platinum-group elements and gold within the Vourinos chromitite ores, Greece. Economic Geology 86, 1672–1682.

Kovács, G.P., Buda, G., Watkinson, D.H., Tompa, L., 1997. Chromite deposits of the Sagua-Baracoa range, eastern Cuba. Acta Geological Hungarica [Hungary] 40, 337–353.

Lago, B., Rabinowicz, M., Nicolas, A., 1982. Podiform chromite ore bodies: a genetic model. Journal of Petrology 23, 103–125.

Lázaro, C., García-Casco, A., Neubaurer, F., Rojas-Agramonte, Y., Kröner, A., Iturralde-Vinent, M.A., 2009. Fifty-five-million-year history of oceanic subduction and exhumation at the northern ege of the Caribben plate (Sierra del Convento mélange, Cuba). Journal of Metamorphic Geology 27, 19–40.

Leblanc, M., 1995. Chromite and ultramafic rock compositional zoning through a paleotransform fault, Poum, New Caledonia. Economic Geology 90, 2028–2039.

Leblanc, M., Ceuleneer, G., 1992. Chromite crystallization in a multicellular magma flow: evidence from a chromitite dike in the Oman ophiolite. Lithos 27, 231–257.

Please cite this article as: González-Jiménez, J.M., et al., High-Cr and high-Al chromitites from the Sagua de Tánamo district, Mayarí-Cristal ophiolitic massif (eastern Cuba): Constraints on..., Lithos (2011), doi:10.1016/j.lithos.2011.01.016

Leblanc, M., Violette, J.F., 1983. Distribution of aluminum-rich and chromium-rich chromite pods in ophiolite peridotites. Economic Geology 78, 293–301.
Lorand, J.P., Alard, O., Luguet, A., 2010. Platinum-group element micronuggets and refertilization process in Lherz orogenic peridotite (northeastern Pyrenees, France). Earth and Planetary Science Letters 289, 298–310.
Lorand, J.P., Pattou, L., Gros, M., 1999. Fractionation of platinum-group elements and gold in the upper mantle: a detailed study in Pyrenean orogenic lherzolites. Journal of Petrology 40, 957–981.
Luguet, A., Alard, O., Lorand, J.P., Pearson, N.J., Ryan, C., O'Reilly, S.Y., 2001. Laser-ablation microprobe (LAM)-ICPMS unravels the highly siderophile element geochemistry of the ocean mantle. Earth and Planetary Science Letters 189, 285–294.
Malitch, K.N., Melcher, F., Mühlhans, H., 2001. Palladium and gold mineralization in podiform chromitite at Kraubath, Austria. Mineralogy and Petrology 73, 247–277.
Marchesi, C., Garrido, C.J., Boch, D., Proenza, J.A., Gervilla, F., Monié, P., Rodríguez-Vega, A., 2007. Geochemistry of cretaceous magmatism in eastern Cuba: recycling of North American continental sediments and implications for subduction polarity in the greater Antilles paleo-arc. Journal of Petrology 48 (9), 1813–1840.
Marchesi, C., Garrido, C.J., Godard, M., Proenza, J.A., Gervilla, F., Blanco-Moreno, J., 2006. Petrogenesis of highly depleted peridotites and gabbroic rocks from the Mayarí-Baracoa Ophiolitic Belt (eastern Cuba). Contributions to Mineralogy and Petrology 151, 717–736.
Marchesi, G., González-Jiménez, J.M., Gervilla, F., Garrido, C.J., Griffin, W.L., O'Reilly, S.Y., Proenza, J.A., Pearson, N.J., 2010. In Situ Re-Os Isotopic Analysis of Platinum-Group Minerals from the Mayarí-Cristal Ophiolitic Massif (Mayarí-Baracoa Ophiolitic Belt, Eastern Cuba): Implications for the Origin of Os-isotope Heterogeneities in Podiform Chromitites. Contributions to Mineralogy and Petrology. doi:10.1007/S00410-010-0575-2.
Matsumoto, I., Arai, S., 2001. Morphological and chemical variations of chromian spinel in dunite–harzburgite complexes from the Sagun zone (SW Japan): implications form mantle/melt reaction and chromitite formation processes. Mineralogy and Petrology 73, 305–323.
Matsumoto, I., Arai, S., Yamauchi, H., 1997. High-Al podiform chromitites in dunite–harzburgite complexes of the Sangun zone, central Chugoku district, Southwest Japan. Journal of Asian Earth Sciences 15, 295–302.
Matveev, S., Ballhaus, C., 2002. Role of water in the origin of podiform chromitite deposits. Earth and Planetary Science Letters 203, 235–243.
Maurel, C., Maurel, P., 1982. Étude expérimentale de la distribution de l'aluminium entre bain silicaté basique et spinelle chromifère. Implications pétrogénétiques : teneur en chrome des spinelles. Bulletin de Minéralogie 105, 197–202.
McElduff, B., Stumpfl, E.F., 1991. The chromite deposits of the Troodos Complex, Cyprus — evidence for the role of a fluid phase accompanying chromite formation. Mineralium Deposita 26, 307–318.
Melcher, F., Stumpfl, E.F., Distler, V., 1994. Chromite deposits of the Kempirsai massif, southern Urals, Kazakhstan. Applied Earth Section B (Transactions Institution Mining and Metallurgy) 103, B87–B162.
Melcher, F., Grum, W., Simon, G., Thalhammer, T.V., Stumpfl, E.F., 1997. Petrogenesis of the ophiolitic giant chromite deposits of Kempirsai, Kazakhstan: a study of solid and fluid inclusions in chromite. Journal of Petrology 38, 1419–1458.
Melcher, F., Grun, W., Thalhammer, T.V., Thalhammer, O.A.R., 1999. The giant chromite deposits at Kempirsai, Urals: constrains from trace elements (PGE, REE) and isotope data. Mineralium Deposita 34, 250–272.
Metfcal, R.V., Shervais, J.W., 2008. Suprasubduction-zone ophiolites: is there really an ophiolite conumdrum? GSA Special Paper: Ophiolites, Arcs, and Batholiths: A tribute to Cilff Hopson, Wrhigth, J.E., and Shervais, J.W. Geological Society of America 438, 191–222.
Mondal, S.K., Ripley, E.M., Li, C., Frei, R., 2006. The genesis of Archaean chromitites from the Nuasahi and Sukinda massifs in the sighbum Craton, India. Precambrian Research 148, 45–66.
Mudholkar, A.A., Paropkari, A.L., 1999. Evolution of the basalts from three back-arc basins of southwest Pacific. Geo-Marine Letters 18, 305–314.
Mungall, J.E., 2002. A Model of Coprecipitation of Platinum-Group Minerals with Chromite from Silicate Melts. 9th International Platinum Symposium, Abstract with Program, Billings, Montana, pp. 321–324.
Mungall, J.E., 2005. Magmatic Geochemistry of the Platinum-Group Elements. Exploration from Platinum-Group Elements Deposits: Short Course Series-Mineralogical Asociation of Canada, vol. 35, pp. 1–34.
Murashko, V.I., Lavandero, R.M., 1989. Chromite in hyperbasite belt of Cuba. International Geology Review 31, 90–99.
Mukherjee, R., Mondal, S.K., Rosing, M.T., Frei, R., 2010. Compositional variations in the Mesoarchean chromites of the Nuggighalli schist belt, Western Dharwar Craton (India): potential parental melts and implications for tectonic setting. Contributions to Mineralogy and Petrology doi:10.1007/s0004-010-0511-5.
Naldrett, AJ., Duke, J.M., 1980. Pt metals in magmatic sulfide ores. Science 208, 1417–1424.
Pagé, P., Barnes, S.-J., 2009. Using trace elements in chromites to constrain the origin of podiform chromitites in the Thetford mines ophiolite, Québec, Canada. Economic Geology 104, 997–1018.
Peng, G., Lewis, J., Lipin, B., McGee, J., Bao, P., Wang, X., 1995. Inclusions of phlogopite and phlogopite hydrates in chromite from the Hongguleleng ophiolite in Xinjang, northwest China. American Mineralogist 80, 1307–1316.
Prichard, H.M., Neary, C.R., Fisher, P.C., O'Hara, M.J., 2008. PGE-rich podiform chromitites in the Al 'Ays ophiolite complex, Saudi Arabia: an example of critical mantle melting to extract and concentrate PGE. Economic Geology 103 (7), 1507–1529.
Prichard, H., Neary, C., Potts, P.J., 1986. Platinum Group Minerals in the Shetland Ophiolite. In: Gallagher, M.J., Ixer, R.A., Neary, C.R., Prichard, H.M. (Eds.), Metallogeny of Basic and Ultrabasic Rocks. The institution of Mining and Metallurgy, London, U.K, pp. 395–414.
Proenza, J.A., Alfonso, P., Melgarejo, J.C., Gervilla, F., Tritlla, J., Fallick, A.E., 2003. D, O and C isotopes in podiform chromitites as fluid tracers for hydrothermal alteration processes of the Mayarí-Baracoa Ophiolitic Belt, eastern Cuba. Journal of Geochemical Exploration 78–79, 1–6.
Proenza, J.A., Díaz-Martínez, R., Iriondo, A., Marchesi, C., Melgarejo, J.C., Gervilla, F., Garrido, C.J., Rodríguez-Vega, A., Lonzano-Santacruz, R., Blanco-Moreno, J., 2006. Primitive Cretaceous island-arc volcanic rocks in eastern Cuba: the Téneme Formation. Geological Acta 4, 103–121.
Proenza, J.A., Gervilla, F., Melgarejo, J.C., Bodinier, J.L., 1999. Al- and Cr-rich chromitites from the Mayarí-Baracoa Ophiolitic Belt (Eastern Cuba): consequence of interaction between volatile-rich melts and peridotites in suprasubduction mantle. Economic Geology 94, 547–566.
Proenza, J.A., Ortega-Gutiérrez, F., Camprubí, A., Tritlla, J., Elías-Herrera, M., Reyes-Salas, M., 2004. Paleozoic serpentinite enclosed chromitites from Tehuitzingo, (Acatlán Complex, southern Mexico): a petrological and mineralogical study. Journal of South American Earth Sciences 16, 649–666.
Proenza, J.A., Zaccarini, F., Escayola, M., Cábana, C., Shalamuk, A., Garuti, G., 2008. Composition and textures of chromite and platinum-group minerals in chromitites of the western ophiolitic belt from Córdoba Pampeans Ranges, Argentine. Ore Geology Review 33, 32–48.
Proenza, J.A., Zaccarini, F., Lewis, J.F., Longo, F., Garuti, G., 2007. Chromian spinel composition and the platinum-group minerals of the PGE-rich Loma Peguera chromitites, Loma Caribe peridotite, Dominican Republic. Canadian Mineralogist 45, 631–648.
Quick, J.E., 1981. The origin and significance of large, tabular dunite bodies in the Trinity Peridotite, northern California. Contributions to Mineralogy and Petrology 78, 413–422.
Quick, J.E., Gergory, R.T., 1995. Significance of melt-wall rock reaction: a comparative anatomy of three ophiolites. Journal of Geology 103, 187–198.
Rammlmair, D., Raschka, H., Steiner, L., 1987. Systematics of chromitite occurrences in Central Palawan, Philippines. Mineralium Deposita 22, 190–197.
Roberts, S., Neary, C.R., 1993. Petrogenesis of Ophiolitic Chromitite. In: Prichard, H.M., Alabaster, T., Harris, N.B.W., Neary, C.R. (Eds.), Magmatic Processes and Plate Tectonics: Geological Society of London, Special Publication, vol. 76, pp. 257–272.
Rollinson, 2005. Chromite in the mantle section of the Oman ophiolite: a new genetic model. The Island Arc 14, 542–550.
Rollinson, P., 2008. The geochemistry of mantle chromitites from the northern part of the Oman ophiolite: inferred parental melt compositions. Contributions to Mineralogy and Petrology 156, 273–288.
Stockman, H.W., Hlava, P.F., 1984. Platinum-group minerals in Alpine chromitites form south-western Oregon. Economic Geology 79, 491–508.
Thalhammer, O.A.R., Prochaska, W., Mühlhans, H.W., 1990. Solid inclusions in chrome-spinels and platinum group element concentrations from the Hochgrössen and Kraubath ultramafic massif (Austria). Contributions to Mineralogy and Petrology 105, 66–80.
Thayer, T.P., 1942. Chrome resources of Cuba. U.S. Geological Survey 935-A, 1–74.
Thayer, P.T., 1964. Principal features and origin of podiform chromite deposits, and some observations on the Guleman-Soridag district, Turkey. Economic Geology 59, 1497–1524.
Tarkian, M., Prichard, H.M., 1987. Irarsite-hollingworthite Ru-, Os–Ir and Rh-bearing PGM's from the Shetland Ophiolite Complex. Mineralium Deposita 22, 178–184.
Tsoupas, G., Economou-Eliopoulos, M., 2008. High PGE contents and extremely abundant PGE-minerals hosted in chromitites from the Veria ophiolite complex, northern Greece. Ore Geology Review 33, 3–19.
Toramaru, A., Fuji, N., 1986. Connectivity of melt phase in a partially molten peridotite. Journal of Geophysical Research 91, 9239–9252.
Uysal, I., Tarkian, M., Sadıklar, M.B., Sen, C., 2007. Platinum group-element geochemistry and mineralogy of ophiolitic chromitites from the Kop Mountains, Northeastern Turkey. Canadian Mineralogist 45, 355–377.
Uysal, I., Tarkian, M., Sadiklar, M.B., Zaccarini, F., Meisel, T., Garuti, G., Heidrich, S., 2009a. Petrology of Al- and Cr-rich ophiolitic chromitites from the Muğla, SW Turkey: implications from composition of chromite, solid inclusions of platinum-group mineral, silicate, and base-metal mineral, and Os-isotope geochemistry. Contributions to Mineralogy and Petrology 158 (5), 659–674.
UysaL, I., Zaccarini, F., Sadiklar, M.B., Tarkian, M., Bernhardt, H.-J., BIGI, S., Garuti, G., 2009b. Occurrence of rare Ru–Fe–Os–Ir-oxide and associated platinum-group minerals (PGM) in the chromitite of Mugla ophiolite, SW-Turkey. Neues Jahrbuch fur Mineralogie 185, 323–333.
Vailler, T., Jenner, G.A., Frey, F.A., Gill, J.B., Davis, A.S., Volpe, A.M., Hawkins, J.W., Morris, J.D., Cawood, P.A., Morton, J.L., Scholl, D.W., Rautenshlein, M., White, W.M., Williams, M., 1991. Subalkaline andesites from Valu Fa Ridge, a back-arc spreading center in southern Lau Basin: petrogenesis, comparative chemistry and tectonic implications. Chemical Geology 91, 227–256.
Wilson, M., 1989. Igneous Petrogenesis. Unwin Hyman, London. pp 446.
Zaccarini, F., Proenza, J.A., Ortega-Gutiérrez, F., Garuti, G., 2005. Platinum group minerals in ophiolitic chromitites from Tehuitzingo (Acatlan Complex, Southern Mexico): implications for postmagmatic modification. Mineralogy and Petrology 84, 147–168.
Zaccarini, F., Garuti, G., Proenza, J.A., Campos, L., Thalhammer, O.A.R., Aiglsperger, T., Lewis, J., in press. Chromite and platinum-group-elements mineralization in the Santa Elena ophiolitic ultramafic nappe (Costa Rica): geodynamic implications. Geologica Acta.
Zhou, M.F., Bai, W.J., 1992. Chromite deposits in China and their origin. Mineralium Deposita 27, 192–199.

Please cite this article as: González-Jiménez, J.M., et al., High-Cr and high-Al chromitites from the Sagua de Tánamo district, Mayarí-Cristal ophiolitic massif (eastern Cuba): Constraints on..., Lithos (2011), doi:10.1016/j.lithos.2011.01.016

Zhou, M.F., Robinson, P.T., 1994. High-Cr and high-Al podiform chromitites, Western China: relationships to partial melting and melt/rock reaction in the upper mantle. International Geology Review 36, 678–686.
Zhou, M.F., Robinson, P.T., 1997. Origin and tectonic environment of podiform chromite deposits. Economic Geology 92, 259–262.
Zhou, M.F., Robinson, P.T., Bai, W.J., 1994. Formation of podiforme chromites by melt–rock interaction in the upper mantle. Mineralium Deposita 29, 98–101.
Zhou, M.F., Robinson, P.T., Malpas, J., Zijin, L., 1996. Podiform chromites in the Luobusa Ophiolite (Southern Tibet): implications for melt–rock interaction and chromite segregation in the upper mantle. Journal of Petrology 37, 3–21.
Zhou, M.F., Keays, R.R., Kerrich, R.W., 1998. Controls on platinum-group elemental distributions of podiform chromitites: a case study of high-Cr and high-Al chromitites from Chinese orogenic belt. Geochimica et Cosmochimica Acta 62, 677–688.

Please cite this article as: González-Jiménez, J.M., et al., High-Cr and high-Al chromitites from the Sagua de Tánamo district, Mayarí-Cristal ophiolitic massif (eastern Cuba): Constraints on..., Lithos (2011), doi:10.1016/j.lithos.2011.01.016